FFI RAPPORT

PERFORATION OF CONCRETE TARGETS

SJØL Henrik, TELAND Jan Arild

FFI/RAPPORT-2001/05786

FFIBM/766/130

Approved
Kjeller 6. August 2003

Bjarne Haugstad
Director of Research

PERFORATION OF CONCRETE TARGETS

SJØL Henrik, TELAND Jan Arild

FFI/RAPPORT-2001/05786

FORSVARETS FORSKNINGSINSTITUTT
Norwegian Defence Research Establishment
P O Box 25, NO-2027 Kjeller, Norway

FORSVARETS FORSKNINGSINSTITUTT (FFI)
Norwegian Defence Research Establishment

P O BOX 25
N0-2027 KJELLER, NORWAY

UNCLASSIFIED

SECURITY CLASSIFICATION OF THIS PAGE
(when data entered)

REPORT DOCUMENTATION PAGE

1) PUBL/REPORT NUMBER	2) SECURITY CLASSIFICATION	3) NUMBER OF PAGES
FFI/RAPPORT-2001/05786	UNCLASSIFIED	48
1a) PROJECT REFERENCE	**2a) DECLASSIFICATION/DOWNGRADING SCHEDULE**	
FFIBM/766/130	-	

4) TITLE

PERFORATION OF CONCRETE TARGETS

5) NAMES OF AUTHOR(S) IN FULL (surname first)

SJØL Henrik, TELAND Jan Arild

6) DISTRIBUTION STATEMENT

Approved for public release. Distribution unlimited. (Offentlig tilgjengelig)

7) INDEXING TERMS

IN ENGLISH:	IN NORWEGIAN:
a) Perforation	a) Perforasjon
b) Concrete	b) Betong
c) Cavity expansion theory	c) Hulromsekspansjonsteori
d) Residual velocity	d) Resthastighet
e) Ballistic limit	e) Ballistisk grense

THESAURUS REFERENCE:

8) ABSTRACT

During construction of concrete buildings for military purposes, one is interested in minimizing the potensial damage caused by an impacting projectile. To achieve this, it is necessary to use a wall thickness that either stops the projectile from perforating the structure, or at least reduces the residual velocity considerably. In this report, a new analytical approach for calculating the penetration process of a rigid projectile in a finite structure is presented. The method is based on cavity expansion theory and uses a force reduction factor to decrease the force on the projectile when it is close to the rear side of target, giving a more realistic expression for the force. Both ballistic limit, residual velocity and required wall thickness to prevent perforation can be determined from the model. On comparison with experimental data, the new model gives good agreement and is seen as a vast improvement over existing empirical models. Using the new method together with the models for semi-infinite targets, we have a complete collection of powerful analytical tools for analysing normal impact of rigid projectiles against concrete targets.

9) DATE	AUTHORIZED BY	POSITION
	This page only	
6. August 2003	Bjarne Haugstad	Director of Research

ISBN-82-464-0760-0

UNCLASSIFIED

SECURITY CLASSIFICATION OF THIS PAGE
(when data entered)

PERFORATION OF CONCRETE TARGETS

1 INTRODUCTION

For design and construction of concrete buildings for military purposes, it is necessary to know the required wall thickness to prevent perforation of a given projectile. Therefore a lot of different work has been performed on penetration into concrete. In Teland [1], several existing empirical formulas for predicting penetration, spalling or perforation of concrete targets were analysed. The main focus was, however, penetration into semi-infinite targets. In Forrestal et al [2], cavity expansion theory (CET) was used to calculate the final penetration depth into semi-infinite targets, an approach that was further developed by Sjøl & Teland [3], and Teland & Sjøl [4].

However, for real constructions, the thickness of the walls, or the concrete cover, are indeed finite. An important question is therefore to determine the required thickness to prevent perforation or spalling. In this report, the problem of determining the perforation thickness and even the residual velocity will be analysed.

In [3,4], the penetration model based on cavity expansion theory was analysed using non-dimensional parameters. The existing empirical models reviewed in [1] will here be analysed using the same non-dimensional parameters in order to compare these empirical models with the analytical expressions.

Littlefield et al [5] used CET to determine the target resistance in steel targets with small diameters (boundary effects). In Teland & Sjøl [6] and Sjøl & Teland [7], the same method was applied for thick concrete targets to give an estimate of the redused force on the penetrator. In the present paper, this approach is further developed to be applicable for thin targets as well.

The new theory will be compared to other available models from the literature and different experimental data.

2 APPLICATION OF CAVITY EXPANSION THEORY

In this chapter we briefly review the use of CET for determining the penetration depth into semi-infinite targets, and how boundary effects can be taken into account. This theory will then be extended to determine the force acting on a projectile reaching the rear side of the target, resulting in analytical formulas for residual velocity, ballistic limit velocity, thickness to prevent perforation and finally penetration depth into thin targets.

Two different cavity expansion (CE) models can be used, namely spherical and cylindrical models. In spherical CE, the cavity expands spherically, and spherical symmetry can be used in the calculations. In cylindrical CE, the "cylinder" expands in the radial direction, while the length of the cylinder is assumed to be infinite. It is, however, not obvious what is the best approach in perforation problems. Therefore, we have analysed both spherical and cylindrical CE in this report.

In Figure 2.1 we have shown the most important geometrical parameters that are used in the theoretical analysis.

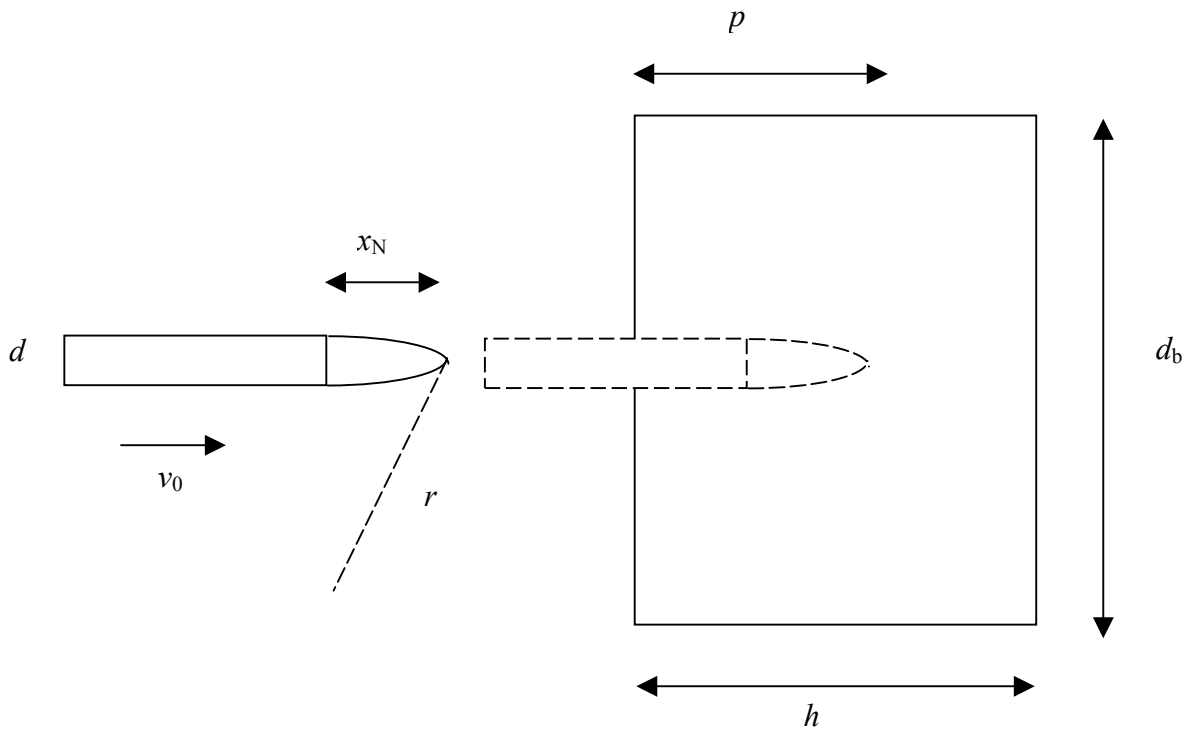

Figure 2.1 Description of penetration problem.

The variables used in the analysis are as follows. Some of them are also defined in Figure 2.1.

d = Projectile diameter
d_t = Target diameter
f = Force acting on projectile nose
h = Target thickness
m = Projectile mass
p = Final penetration depth
r = Projectile nose radius
x_N = Length of projectile nose
ρ_t = Target density
σ_c = Target compressive strength

From these parameters, it is convenient to define the following non-dimensional quantities:

$$F = \frac{f}{\sigma_c d^2}$$

$$H = \frac{h}{d}$$

$$M = \frac{m}{d^3 \rho_t}$$

$$P = \frac{p}{d}$$

$$S = 49.5\sigma_c^{-0.43}$$

$$V = \sqrt{\frac{m}{d^3 \sigma_c}} v$$

2.1 Semi-infinite targets (Forrestal's formula)

In Forrestal's CET approach, the penetration process is divided into two different phases. In the cratering phase, the projectile nose is not yet fully embedded in the target and the force is assumed proportional to the current penetration depth. In the tunnelling phase, the entire projectile nose is inside the target, and the force is determined from CET.

The force acting on the projectile can then be written as:

$$F_0 = \begin{cases} C_\infty X & X \le X_N \\ \frac{\pi}{4} S \left(1 + \frac{N}{M} \frac{V^2}{S} \right) & X \ge X_N \end{cases} \qquad (2.1)$$

where C_∞ is a constant determined by continuity in force, displacement and velocity, and is found to be

$$C_\infty = \frac{\pi S}{4X_N} \frac{\frac{M}{N} + \frac{V_0^2}{S}}{\frac{M}{N} + \frac{\pi X_N}{4}} \tag{2.2}$$

Since the projetile is assumed rigid, Newton's 2nd law can now be used to determine the deceleration of the projectile:

$$\frac{\partial^2 X}{\partial T^2} = V \frac{\partial V}{\partial X} = -F_0 \tag{2.3}$$

After integration of Equation (2.3), the final penetration depth is found to be [3]:

$$P_\infty = \frac{2}{\pi} \frac{M}{N} \ln\left(\frac{V^2/S + M/N}{M/N + X_N (\pi/4)} \right) + X_N \tag{2.4}$$

In [4], Equation (2.4) is generalized for projectiles with truncated noses. Such projectiles will not be analysed in this report since there is very little experimental data available.

2.2 Boundary effects

For small target diameters, the force on the projectile will be reduced due to boundary effects. This is accounted for mathematically by introducing a correction factor α, depending on the target diameter, but constant during the penetration process.

$$F = \alpha(d_i/d) F_0(V) \quad X \geq X_N \tag{2.5}$$

The correction factor α is further discussed in Chapter 3 for different material models. However, on assuming a constant value of α, the final penetration depth is given by

$$P_\infty = \frac{1}{\alpha} \frac{2}{\pi} \frac{M}{N} \ln\left(\frac{V^2/S + M/N}{M/N + \alpha X_N (\pi/4)} \right) + X_N \tag{2.6}$$

The boundary effect problem is further discussed in [5,6].

2.3 Thin targets

For thin targets, i.e. in situations where the projectile perforates or almost perforates the target, we have another boundary effect involved. In the situation described in Section 2.2, the distance to the free surface was assumed to be constant resulting in a constant correction factor. However, as the projectile approaches the rear side of the target, the distance to the free surface is reduced, and the correction factor should also be influenced by this fact. To proceed further, it is convenient to divide the process into several phases.

In the beginning of the penetration process, the projectile is not affected by any reflections from the rear side. Hence the target resistance will be the same as for penetration into semi-infinite targets. However, as soon as pressure waves from the projectile have been reflected by the rear surface and travelled back to the projectile, a different situation arises. The projectile is then (in some way) influended by the reflected waves, resulting in a reduced target resistance.

The mathematical problem is then reduced to two different cases, depending on whether the reflected waves return to the projectile before or after the nose has fully penetrated the target

2.3.1 The waves are reflected before the nose has penetrated the target

As for semi-infinite targets, the target resistance is assumed proportional to the current penetration depth as long as the projectile is not fully embedded in the target, while afterwards we use CET to determine the target resistance. The possibilities are summed up in the Table 2.1.

Table 2.1 Definition of the different phases and integration limits in perforation process.

Phase	**Description**	**Force (F)**	**Integration limits**	
			Pen depth	**Velocity**
Phase (i)	"Infinite target"	$C_\infty X$	0 to X_1	V_0 to V_1
Phase (ii)	Corrected cratering phase	$\alpha(X)\cdot C_\infty X$	X_1 to X_2	V_1 to V_2
Phase (iii)	Corrected tunnelling phase	$\alpha(X)\cdot F_0(V)$	X_2 to X_3 (X_3 is P or H)	V_2 to V_3 (V_3 is 0 or V_{exit})

The problem is normally solved "backwards", i.e. starting with phase (iii), and then using phase (i) and (ii) to find the relationships between the different transition velocities. In phase (iii), Newton's 2nd law gives us

$$V\frac{\partial V}{\partial X} = -\alpha(X)\cdot F_0(V) \tag{2.7}$$

Integration of Equation (2.7) gives

$$\int_{X_2}^{X_3} \alpha(X)dX = \frac{2}{\pi}\frac{M}{N}\left[\ln\left(1+\frac{N}{M}\frac{V_2^2}{S}\right)-\ln\left(1+\frac{N}{M}\frac{V_3^2}{S}\right)\right] \tag{2.8}$$

From phase (ii) we have

$$V\frac{\partial V}{\partial X} = -\alpha(X)\cdot C_\infty X \tag{2.9}$$

which integrates to

$$V_1^2 - V_2^2 = 2C_\infty \int_{X_1}^{X_2} X\alpha(X)dX \tag{2.10}$$

In phase (i), Newton's 2nd law gives

$$V\frac{\partial V}{\partial X} = -C_\infty X \tag{2.11}$$

Integration gives

$$V_0^2 - V_1^2 = C_\infty X_1^2 \tag{2.12}$$

Combining Equations (2.10) and (2.12) gives the following relationship between V_0 and V_2.

$$V_2^2 = V_0^2 - C_\infty \left[X_1^2 + 2\int_{X_1}^{X_2} X\alpha(X)dX \right] \tag{2.13}$$

Inserting (2.13) into (2.8) result in an equation where we apparently have two unknown parameters, V_3 and X_3. But since either X_3 or V_3 is fixed, Equation (2.8) can be used to determine the residual velocity or the penetration depth.

The ballistic limit velocity is found by setting $X_3 = H$ and $V_3 = 0$, and solving Equation (2.8) with respect to V_0. Finally, the thickness to prevent perforation is also found by setting $X_3 = H$ and $V_3 = 0$, but in this case the problem is somewhat more complicated, as the correction factor α also depends on the target thickness. This problem must therefore be solved numerically.

2.3.2 The nose has penetrated the target before the waves are reflected

Table 2.2 Definition of the different phases and integration limits in perforation process.

Phase	**Description**	**Force (F)**	**Integration limits**	
			Pen depth	**Velocity**
Phase (i)	"Infinite target"	$C_\infty X$	0 to X_1	V_0 to V_1
Phase (ii)	"Infinite tunnelling phase"	$F_0(V)$	X_1 to X_2	V_1 to V_2
Phase (iii)	Corrected tunnelling phase	$\alpha(X)\cdot F_0(V)$	X_2 to X_3 (X_3 is P or H)	V_2 to V_3 (V_3 is 0 or V_{exit})

In Case II, the result from phase (iii) is also determined by Equation (2.8). In phase (ii), Newton's 2nd law is also given by

$$V\frac{\partial V}{\partial X} = -F_0(V) \tag{2.14}$$

Integration of Equation (2.7) gives

$$X_2 - X_1 = \frac{2}{\pi}\frac{M}{N}\left[\ln\left(1+\frac{N}{M}\frac{V_1^2}{S}\right) - \ln\left(1+\frac{N}{M}\frac{V_2^2}{S}\right)\right] \tag{2.15}$$

The relationship between V_0 and V_1 is given by Equation (2.12). On combining Equations (2.12) and (2.15), we obtain the following relationship between V_2 and V_0:

$$V_2^2 = S\frac{M}{N}\left[\exp\left(-\frac{\pi}{2}\frac{N}{M}\left(X_2 - X_1\right)\right)\left\{1+\frac{N}{M}\left(\frac{V_0^2}{S} - \frac{C_\infty}{S}X_1^2\right)\right\} - 1\right] \tag{2.16}$$

2.3.3 Determine X_1 and X_2

To decide which of the cases discussed above that should be applied, we need to estimate the current penetration depth when the reflected pressure waves have returned to the projectile nose. Let the speed of sound in the target material be denoted by c_t, and assume for simplicity that the projectile's velocity is constant in the start of the penetration process. The projectile has then penetrated

$$X_W = \frac{2}{1+{}^{c_t}\!/_{v_0}}L \tag{2.17}$$

into the target when the waves are reflected. For thin targets, which is the subject of this report, the reflected waves normally return to the projectile in the cratering phase, i.e. before the nose is fully embedded in the target[1]. As discussed in the previous sections, X_1 and X_2 are defined as follows:

$$X_1 = \min(X_N, X_W) \qquad X_2 = \max(X_N, X_W) \tag{2.18}$$

3 TARGET RESISTANCE

The only remaining problem now is to find an expression for α as a function of material and geometrical parameters. This calculation is, however, not trivial, and there are in fact several different approaches.

In this chapter, we will adopt the static approach in Littlefield et al [7] for boundary effect problems in Mises materials, as reviewed in Section 3.1. This method is extended in Section 3.2, using a Mohr-Coulomb material model instead, which should be more correct for concrete targets.

Both spherical and cylindrical cavity expansion theory are applied to give an estimate of the correction factor. There is, however, no significant difference in the various methods, as will be shown in the discussions of the theoretical perforation model. The models described in this report are results of static cavity expansion. In Warren and Poormon [8] the target resistance for dynamic problems are calculated, but this model will not be discussed here. The dynamic terms do not contribute significantly to the residual velocity, but should be included in a complete numerical model. The static expressions in this chapter are calculated in detail in Appendix A.

3.1 Mises model

We here present results for both spherical and cylindrical CET with a Mises material model.

3.1.1 Cylindrical cavity expansion

In Littlefield et al [7], the relative target resistance for small targets, using a Mises material model was calculated using cylindrical cavity expansion theory.

$$R_t = \frac{Y}{2}\left[1 - \left(\frac{d_{ep}}{d_t}\right)^2 + \ln\left(\frac{d_{ep}}{d}\right)^2\right] \tag{3.1}$$

[1] For the impact velocities used in the experiments discussed later in this paper, X_W is between 0.1 and 0.3 times the scaled target thickness H. X_W is between 0.2 and 2.1 for the values of scaled target thickness discussed in this paper. In any case, X_W is less than X_N, which is approximately 3 in the experiments discussed in the present paper.One experiment (with v_0 = 1035 m/s) gives $X_W > 3$, but in this case, the impact velocity is far from the ballistic limit.

where

$$\left(\frac{d_{ep}}{d_t}\right)^2 = \frac{1}{2(1-2\nu)}\left[\sqrt{1+\frac{8G}{Y}(1-2\nu)\left(\frac{d}{d_t}\right)^2}-1\right] \tag{3.2}$$

$$R_\infty = \frac{Y}{2}\left(1+\ln(2G/Y)\right) \tag{3.3}$$

The expression for target resistance given in Equation (3.1) assume that we have both plastic and elastic material in the target. If the target diameter is sufficiently small, the plastic zone will extend all the way to the edge. In this case, the elastic-plastic interface does no longer exist, and the formulas need to be modified.

This can be achieved in two different ways. One possibility is to calculate the target resistance using for instance mass conservation in the plastic region, as done in Littlefield et. al [7] for targets with small diameters. However, this gives little contribution when analyzing the rear side of the target in perforation problems, so we will instead use a simpler approach by just setting $d_{ep} = d_t$ in Equation (3.1).

If the elastic-plastic interface reaches the boundary ($d_{ep} = d_t$), the target resistance is then found from

$$\hat{R}_t = \frac{Y}{2}\ln\left(\frac{d_t}{d}\right)^2 \tag{3.4}$$

Substituting d_t with $2(l - x)$, where l is the thickness of the target and x is the current penetration depth, into Equation (3.4), the following expression of the target resistance is then found

$$\hat{\alpha}(x) = \frac{\hat{R}_t}{R_\infty} = \frac{\ln(4(H-X)^2)}{1+\ln(2G/Y)} \tag{3.5}$$

In perforation problems, the projectile is close to the rear side of the concrete target. In this case, the plastic zone in front of the projectile's nose will most likely have reached the rear side of the target. This means that the distance to the free surface is equal to the elastic-plastic radius. Equation (3.4) is therefore used for the target resistance instead of Equation (3.1). If Equation (3.5) predicts $\hat{\alpha}(x) > 1.0$, it is set to 1.0, i.e. the distance to the rear side is sufficiently large to avoid correction in the resistance force.

3.1.2 Spherical cavity expansion

Using spherical cavity expansion theory, the corresponding correction models are as follows:

$$\alpha_t = \frac{1-\left(\frac{d_{ep}}{d_t}\right)+\ln\left\{\left(\frac{d_{ep}}{d_t}\right)^3\right\}+\ln\left\{\left(\frac{d_t}{d}\right)^3\right\}}{1+\ln\left(\frac{2G}{Y}\right)}$$

$$\left(\frac{d_{ep}}{d_t}\right)^3 = \frac{1}{4}\frac{1+\nu}{1-2\nu}\left(\sqrt{1+\frac{16G}{Y}\frac{1-2\nu}{1+\nu}\left(\frac{d}{d_t}\right)^3}-1\right) \tag{3.6}$$

If the elastic-plastic interface reaches the boundary ($d_{ep} = d_t$), the target resistance is found from

$$\alpha_t = \frac{\ln\left\{\left(\frac{d_t}{d}\right)^3\right\}}{1+\ln\left(\frac{2G}{Y}\right)} \tag{3.7}$$

3.2 Mohr-Coulomb model

For concrete, the yield limit is known to depend on the pressure. It is therefore more correct to use a Mohr Coulomb material model to describe such a material. The Mohr-Coulomb material model can be written as

$$Y = Y_0 + \beta p \tag{3.8}$$

In Appendix A, the derivation of the target resistance for MC-materials can be found. Here we just present the results.

3.2.1 Spherical cavity expansion

We obtain using spherical cavity expansion:

$$R_t = \frac{Y_0}{\beta}\left[1-\frac{\left(\frac{d}{d_{ep}}\right)^{2\beta/(1-\frac{2}{3}\beta)}}{1-\frac{2\beta}{3-2\beta}\left(\left(\frac{d_{ep}}{d_t}\right)^3-1\right)}\right] \tag{3.9}$$

where

$$\left(\frac{d}{d_{ep}}\right)^3 = \frac{{}^{3Y_0}\!/_{2G} + 2\beta\left({}^{d}\!/_{d_t}\right)^3 + \sqrt{\left({}^{3Y_0}\!/_{2G} + 2\beta\left({}^{d}\!/_{d_t}\right)^3\right)^2 + 12\,{}^{Y_0}\!/_{K}\left({}^{d}\!/_{d_t}\right)^3}}{6} \tag{3.10}$$

$$R_\infty = \frac{Y_0}{\beta}\left[1 - \frac{3-2\beta}{3}\left(\frac{Y_0}{2G}\right)^{{}^{2\beta}\!/_{(3-2\beta)}}\right] \tag{3.11}$$

In the case where the plastic zone reaches the boundary ($d_{ep} = d_t$), we obtain

$$R_t = \frac{Y_0}{\beta}\left[1 - \left(\frac{d}{d_t}\right)^{{}^{2\beta}\!/_{(1-{}^{2}\!/_{3}\beta)}}\right] \tag{3.12}$$

and if d_t is replaced by *2(l-x)*, the target resistance is again found to be

$$\alpha_{mc} = \frac{1 - \left(2\left[L - X\right]\right)^{-{}^{2\beta}\!/_{(1-{}^{2}\!/_{3}\beta)}}}{1 - \frac{3-2\beta}{3}\left(\frac{Y_0}{2G}\right)^{{}^{2\beta}\!/_{(3-2\beta)}}} \tag{3.13}$$

In the limit $\beta \to 0$, we retrieve the Mises result given in Chapter 3.1.

3.2.2 Cylindrical cavity expansion

We obtain using cylindrical cavity expansion:

$$R_t = \frac{3Y_0}{2\beta}\left[1 - \frac{\left(\frac{d}{d_{ep}}\right)^{{}^{2\beta}\!/_{(3-\beta)}}}{1 - \frac{\beta}{3-\beta}\left(\left(\frac{d_{ep}}{d_t}\right)^2 - 1\right)}\right] \tag{3.14}$$

where

$$\left(\frac{d_{ep}}{d_t}\right)^2 = \frac{-\left[{}^{3Y_0}\!/_{4G} + \beta\left({}^{d}\!/_{d_t}\right)^2\right] + \sqrt{\left({}^{3Y_0}\!/_{4G} + \beta\left({}^{d}\!/_{d_t}\right)^2\right)^2 + 9\,{}^{Y_0}\!/_{G}\left(1-2\nu\right)\left({}^{d}\!/_{d_t}\right)^2}}{{}^{3Y_0}\!/_{2G}\left(1-2\nu\right)} \tag{3.15}$$

$$R_\infty = \frac{2Y_0}{3\beta}\left[1 - \left(3-\beta\right)\left(\frac{Y_0}{4G}\right)^{-{}^{\beta}\!/_{(3-\beta)}}\right] \tag{3.16}$$

In the case where the plastic zone reaches the boundary ($d_{ep} = d_t$), we obtain

$$R_t = \frac{3Y_0}{2\beta}\left[1-\left(\frac{d}{d_t}\right)^{2\beta/(3-\beta)}\right] \tag{3.17}$$

and if d_t is replaced by *2(l-x)*, the target resistance is again found to be

$$\alpha_{mc} = \frac{1-\left(2\left[L-X\right]\right)^{-2\beta/(3-\beta)}}{1-(3-\beta)\left(\frac{Y_0}{4G}\right)^{-\beta/(3-\beta)}} \tag{3.18}$$

Again, we retrieve the Mises result given in Chapter 3.1 in the limit $\beta \to 0$.

3.3 Comparison between target resistance models

In this section we compare the various target resistance models for a specific material.

It is not obvious how to apply the Mises yield strength for concrete materials. The shear modulus (G) is well defined, and Y is here chosen to be the highest level on the Mohr-Coulomb curve. Since only "ln(G/Y)" is included in the mathematical expressions for target resistance, it is expected that α is not very sensitive for the choice of Y. For low strength concrete, we chose G = 3490 MPa and Y = 165 MPa.

For the Mohr-Coulomb model, the target resistance is more sensitive to the choice of Y_0 and b. In [9], a 30 MPa concrete was analysed, and the parameters describing the Mohr-Coulomb model is given in Table 3.1.

Table 3.1 Parameters used to describe the Mohr-Coulomb model.

Pressure [MPa]	Yield stress [MPa]
0	6.69
33	50
120	110
250	165

From Table 3.1, Y_0 = 6.69 and the slope (β) for each interval is found to be 1.31, 0.69 and 0.42, respectively. The extreme cases will be Y_0 = 6.69 and β = 1.31, i.e. the target resistance is determined by the "low pressure region", and Y_0 = 60 and β = 0.42, which means that the "high pressure region" is dominant. The value Y_0 = 60 is determined by extrapolating the straight line in the pressure interval between 120 MPa and 250 MPa to zero pressure. For penetration purposes, it is likely that the "high pressure region" of the Mohr-Coulomb curve determines the result, hence the values Y_0 = 60 and β = 0.42 are chosen.

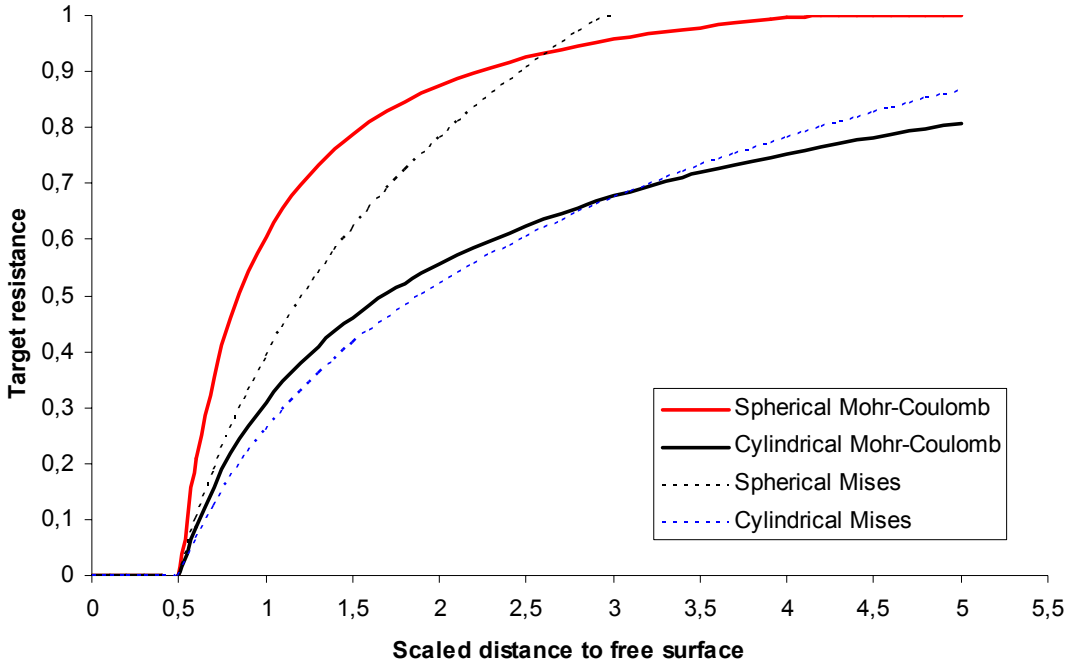

Figure 3.1: Relative target resistance as a function of distance to free surface, for Mises and MC materials.

In Figure 3.1, the target resistance for Mises and MC materials as a function of the distance to the free surface is shown. We see that the main difference is between the spherical and cylindrical CET approaches, not the choice of material model. In the analysis of residual velocity in Chapter 4, the analytical model will be used with both spherical and cylindrical Mohr-Coulomb material models.

4 RESIDUAL VELOCITY

After a projectile has perforated a concrete wall, it will have a residual velocity. Determination of this velocity has been shown to be a rather difficult task, especially near the ballistic limit. However, several empirical relationships between residual velocity and impact velocity exist. The cavity expansion approach presented in this report is compared to some of these formulas, and to a wide range of empirical data.

4.1 Previous work

In several works, experiments have been performed in order to find the relationship between impact and residual velocities. In most cases, this relationship is found by curve fitting the experimental data. The residual velocity can often be written as (see for instance Børvik et al [10])

$$V_{exit} = a\left(V_0^n - V_{bl}^n\right)^{1/n} \tag{4.1}$$

where V_0 is the impact velocity, V_{bl} is the ballistic limit velocity, i.e. the minimum impact velocity required to obtain perforation and a and n are constants. From the Norwegian fortification handbook (1990) [11], Bergman's formula for residual velocity after perforation of fragments into concrete targets can be found:

$$V_{exit} = \left(1 - \frac{H}{P_\infty}\right)^{0.5555} V_0 \tag{4.2}$$

where

$$P_\infty = 8 \cdot 10^{-3} m^{0.4} d^{-1} v_0^{1.8} \sigma_c^{-0.5} \tag{4.3}$$

is the penetration depth into semi-infinite targets. One major drawback with the model in Equation (4.2) is that it predicts no perforation if the target thickness is larger than the penetration depth in a semi-infinite target. This indicates that the model underpredicts the residual velocity. A further discussion is done in Section 4.4.

A modified version of Formula (4.2) can be found in [12]:

$$V_{exit} = \left(1 - \frac{H}{1.239 P_{NDRC} + 1.132}\right)^{0.733} V_0 \tag{4.4}$$

where P_{NDRC} is here calculated from the modified NDRC-formula:

$$P_{\mathrm{NDRC}} = \frac{56,6 \cdot 10^{-6} \left(10^{-9} \cdot {}^{m}\!/_{d^3}\right)^{0,075} N' m v^{1,8}}{d^3 \sigma_{\mathrm{c}}^{\,0,5}} \left(\frac{d}{c}\right)^{0,15} f_{\mathrm{a}} + 1 \tag{4.5}$$

4.2 Cavity expansion approach

Using the cavity expansion approach described in Chapter 2, the residual velocity is also found to be on the form of Equation (4.1) with $p = 2$ and

$$V_{\mathrm{bl}} = \sqrt{S \frac{M}{N} \left[\frac{1}{1-\kappa} \exp\left\{ \frac{\pi}{2} \frac{N}{M} I(X_N, H) \right\} - 1 \right]} \tag{4.6}$$

$$a = \sqrt{(1-\kappa) \exp\left\{ -\frac{\pi}{2} \frac{N}{M} I(X_N, H) \right\}} \tag{4.7}$$

where

$$\kappa = \frac{\pi}{4X_N}\frac{X_1^2 + 2I_x(X_1, X_2)}{M/N + \pi X_N/4}$$

$$I(X_N, H) = \int_{X_N}^{H} \alpha(X)dX \qquad (4.8)$$

$$I_x(X_1, X_2) = \int_{X_1}^{X_2} X\alpha(X)dX$$

The scaled ballistic limit for a 75 mm projectile against concrete targets as a function of scaled target thickness is shown in Figure 4.1.

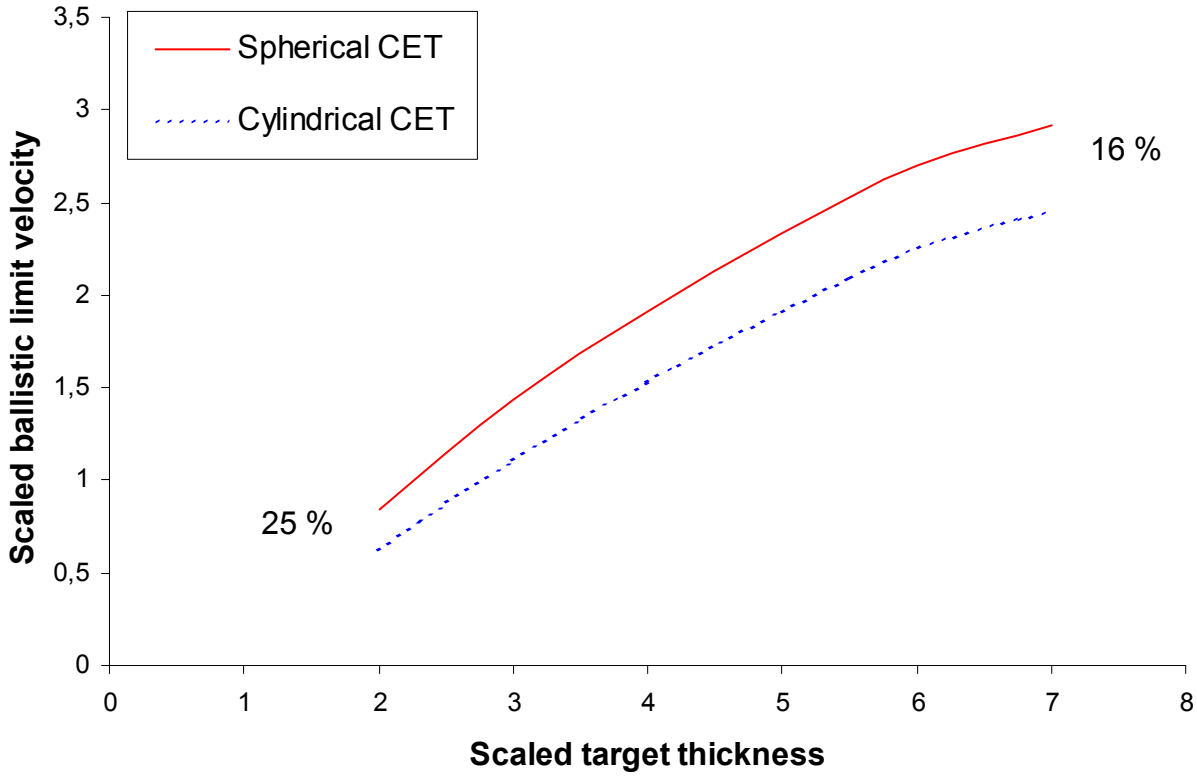

Figure 4.1 *Scaled ballistic limit velocity as a function of scaled target thickness for a 75 mm projectile.*

The deviation in ballistic limit for spherical and cylindrical CET is between 16 % and 25 %.

The scaled mass M depends on the target density. Assuming this is constant, we obtain that

$$v_{bl} \propto \sqrt{S\sigma_c} \propto \sigma_c^{0.285} \qquad (4.9)$$

This means that the ballistic limit velocity increases by a factor 1.5 when the compressive strength is increased by a factor 4. In other words, if a C140 concrete is used instead of a C35

concrete, a projectile must have 50 % higher impact velocity to perforate the same wall thickness.

4.3 Comparison to experiments

Here we will compare the analytical perforation formulas to available experimental data. From Equation (4.1), the scaled residual velocity is a function of the parameters *M/N* and *L*. For a given projectile, the factor *M/N* is (almost) fixed. Therefore, the classification of the different experimental data is made with respect to the scaled target thickness *H*, as shown in Table 4.1. A brief comment is given in each case, i.e. for different target thicknesses. A more detailed discussion is given in Section 4.4.

Table 4.1 Review of all perforation experiments discussed in this report.

H	v_0	v_{exit}	σ_c	Reference
2	135 - 352	0 – 278	200, 600	Darrigade and Buzaud [13]
4	440 – 560	234 - 425	140, 200, 600	Darrigade and Buzaud [13]
4.93	458	187	103	ANNC [14]
5.33	618	287	153	HPC [5]
6	527	20	140	Darrigade and Buzaud [13]
7	301 – 1058	0 – 947	48, 140	Hanchak et. al. [15]

4.3.1 H = 2 (Darrigade and Buzaud [13])

In Darrigade and Buzaud [13], some experiments against high strength concrete were performed. The projectile used in the experiments is shown in Figure 4.2.

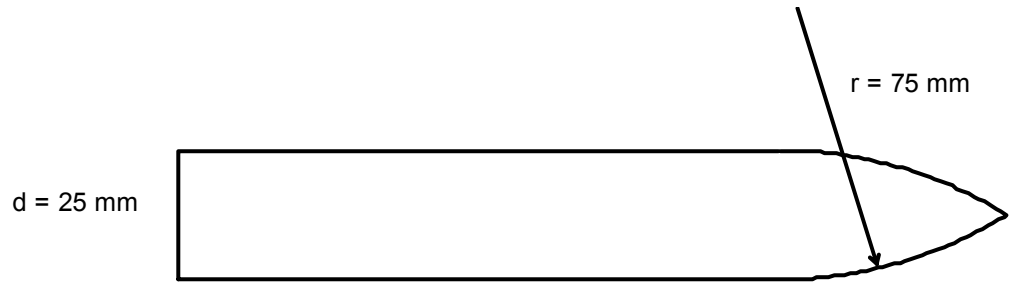

Figure 4.2 The projectile used by Darrigade and Buzaud [13].

Table 4.2 Different experiments against thin concrete targets with H=2 (Darrigade and Buzaud [13]).

Target		Projectile				
Comp str. [MPa]	Thickness [cm]	Mass [kg]	Diameter [mm]	v_0 [m/s]	v_{exit} [m/s]	Remarks
200	56	0.5	25	335	278	
200	55	0.5	25	250	168	
200	50	0.5	25	135	10	
600	50	0.5	25	352	249	
600	52	0.5	25	250	151	
600	53	0.5	25	140	0	

In Figure 4.3, these experiments are compared to the perforation model in this report, and to Bergman's formula and to a model based on the NDRC formula. The FFI-model is shown to agree well with the experiments, while Bergman's model severely underpredicts the residual velocity. This could be due to the fact that the model is mainly designed for fragments, and not for larger projectiles. The NDRC model is better than Bergman's formula, but the FFI-formula gives the best prediction of the residual velocity.

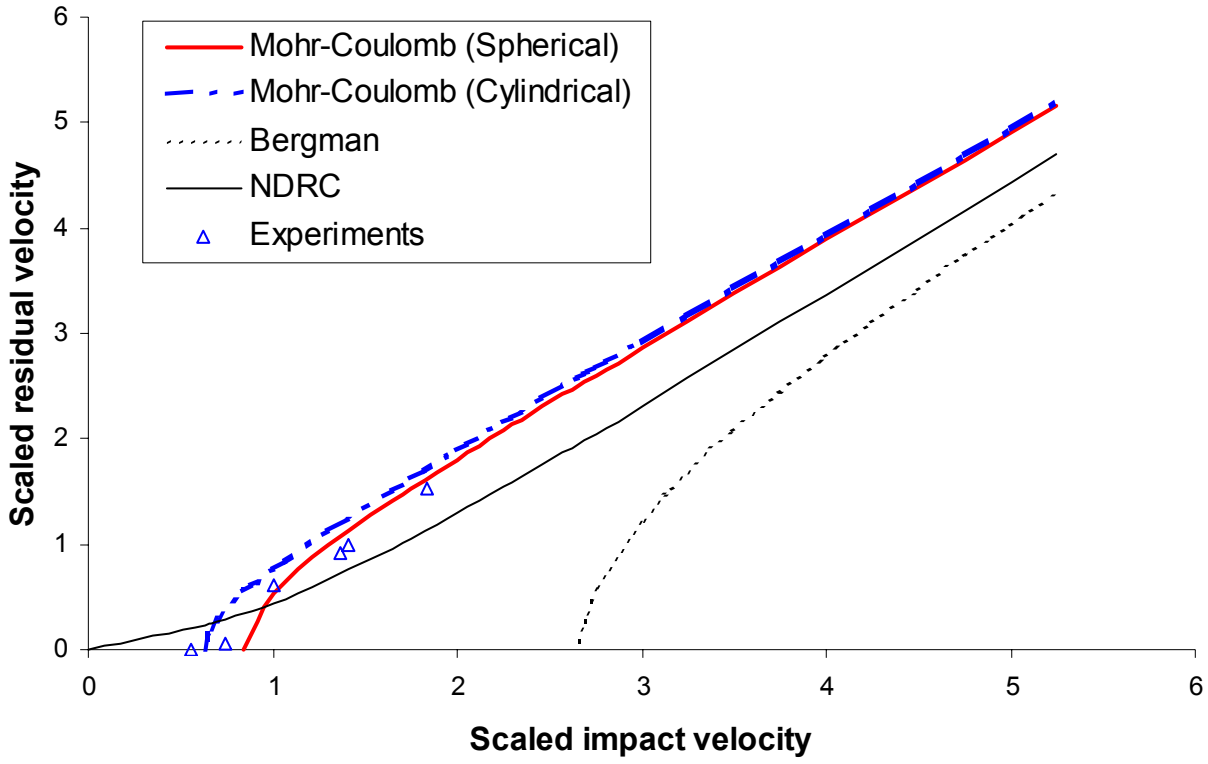

Figure 4.3: Residual velocity as a function of impact velocity for H = 2.

Near the ballistic limit, the experiments seem to be more in agreement with the cylindrical CE model, compared to the spherical CE model. For larger impact velocities, there is little difference between the two CE models, mainly because the target is (very) thin. The CE models are in much better agreement with Bergman's model, and slightly better than the NDRC model.

4.3.2 H = 4 (Darrigade and Buzaud [13])

For $H = 4$, the same projectile, as shown in Figure 4.2 was used in the experiments.

Table 4.3 Different experiments against thin concrete targets with H=4 (Darrigade and Buzaud [13]).

Target		Projectile				
Comp str. [MPa]	Thickness [cm]	Mass [kg]	Diameter [mm]	v_0 [m/s]	v_{exit} [m/s]	Remarks
140	105	0.5	25	545	350	
140	103	0.5	25	445	234	
200	110	0.5	25	550	425	
200	107	0.5	25	445	305	
600	105	0.5	25	560	351	
600	104	0.5	25	440	255	

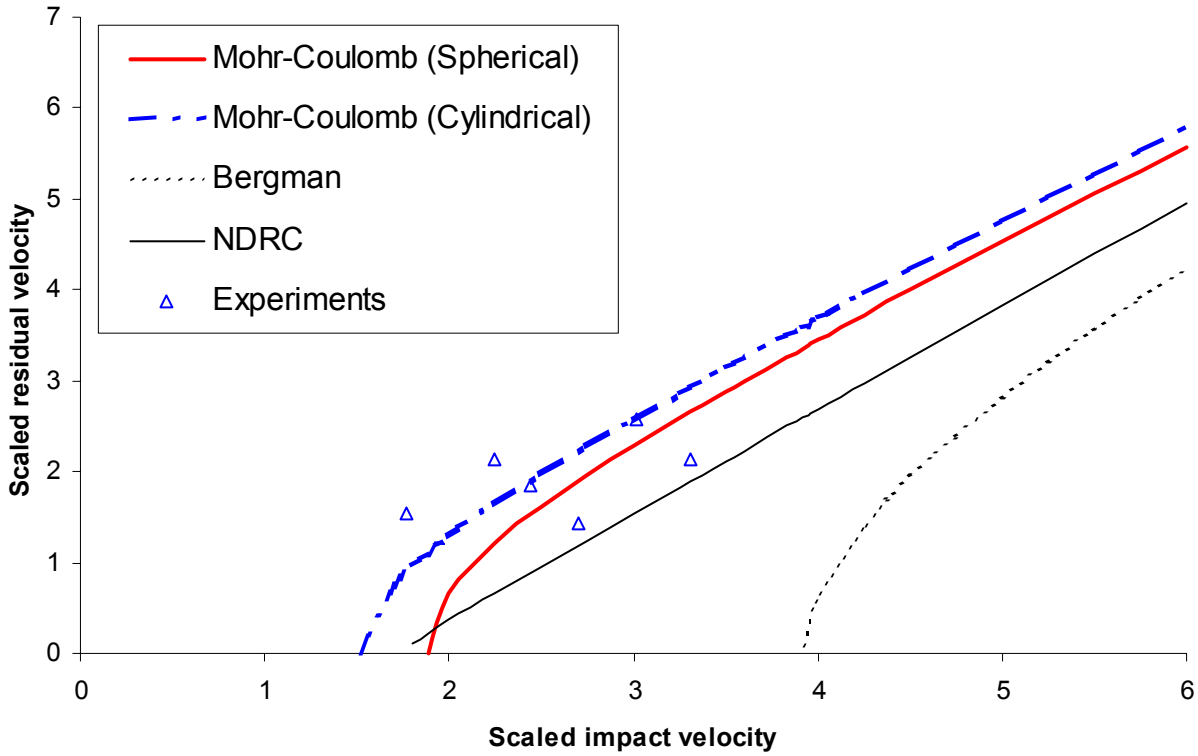

Figure 4.4 Residual velocity as a function of impact velocity for H = 4.

The experiments show some scattering in this case, but compared to the NDRC and Bergman models, the CE approach gives a better agreement to the data.

4.3.3 H = 5 (ANNC [14] and HPC [5,15] experiments)

Figure 4.5 152 mm projectile (left) and 75 mm projectile used in the HPC and ANNC experiments.

Table 4.4 Different experiments against concrete targets with H = 5 (HPC [5,15]/ANNC [14]).

Target		Projectile				
Comp str. [MPa]	Thickness [cm]	Mass [kg]	Diameter [mm]	v0 [m/s]	v_{exit} [m/s]	Remarks
153	40	6.28	75	615	276	Ref. [15]
153	40	6.28	75	618	303	Ref. [15]
153	40	6.28	75	612	293	Ref. [15]
153	40	6.28	75	619	260	Ref. [5]
103	75	44.76	152	460	183	Ref. [14]
103	75	44.76	152	455	204	Ref. [14]
103	75	44.76	152	459	181	Ref. [14]
250	4 x 20	44.76	152	476	Approx. 0	Ref. [5]
36	5 x 20	44.76	152	478	160	Ref. [5]

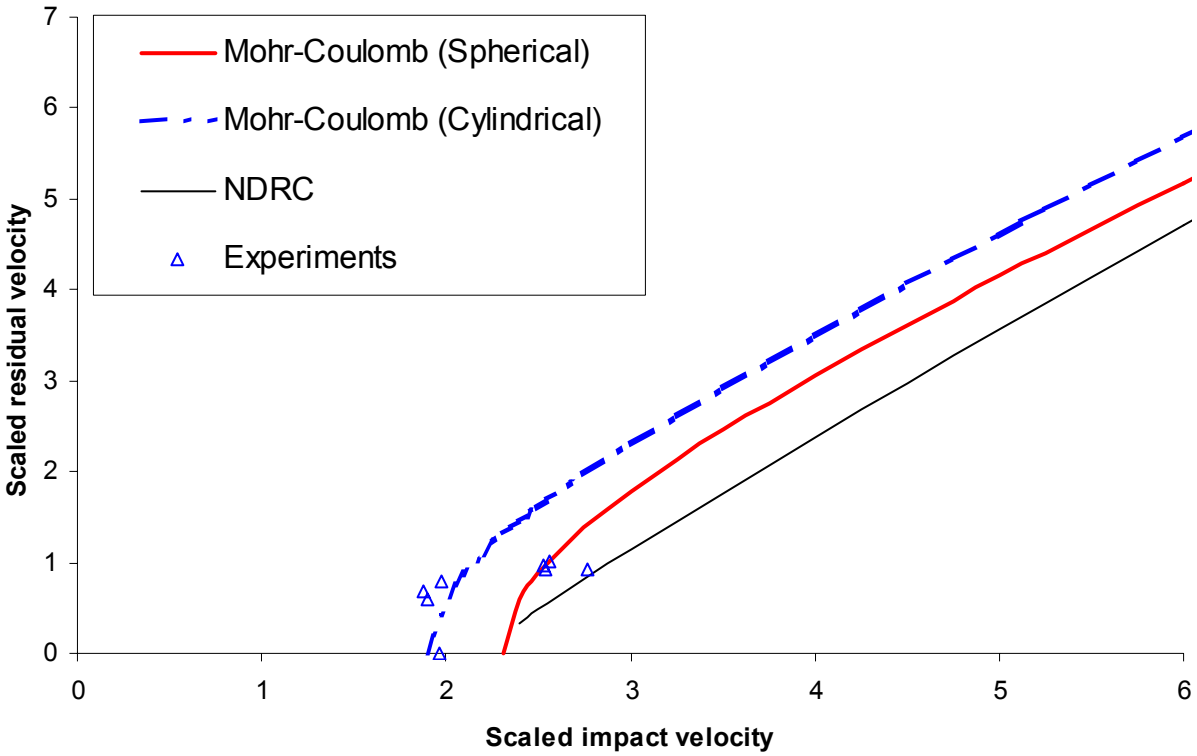

Figure 4.5 Residual velocity as a function of impact velocity for H = 5.

The experiments here are all relatively close to the ballistic limit. The scattering in the data is, however, close to the estimated interval between the spherical and cylindrical CE models.

4.3.4 H = 6 (Darrigade and Buzaud [13])

Table 4.5 Experiment against thin concrete target with H=6 (Darrigade and Buzaud [13]).

Target		Projectile				
Comp str. [MPa]	Thickness [cm]	Mass [kg]	Diameter [mm]	v_0 [m/s]	v_{exit} [m/s]	Remarks
140	156	0.5	25	547	20	

The ballistic limit velocity calculated from the CE model is 364 m/s (cylindrical) and 432 m/s (spherical).

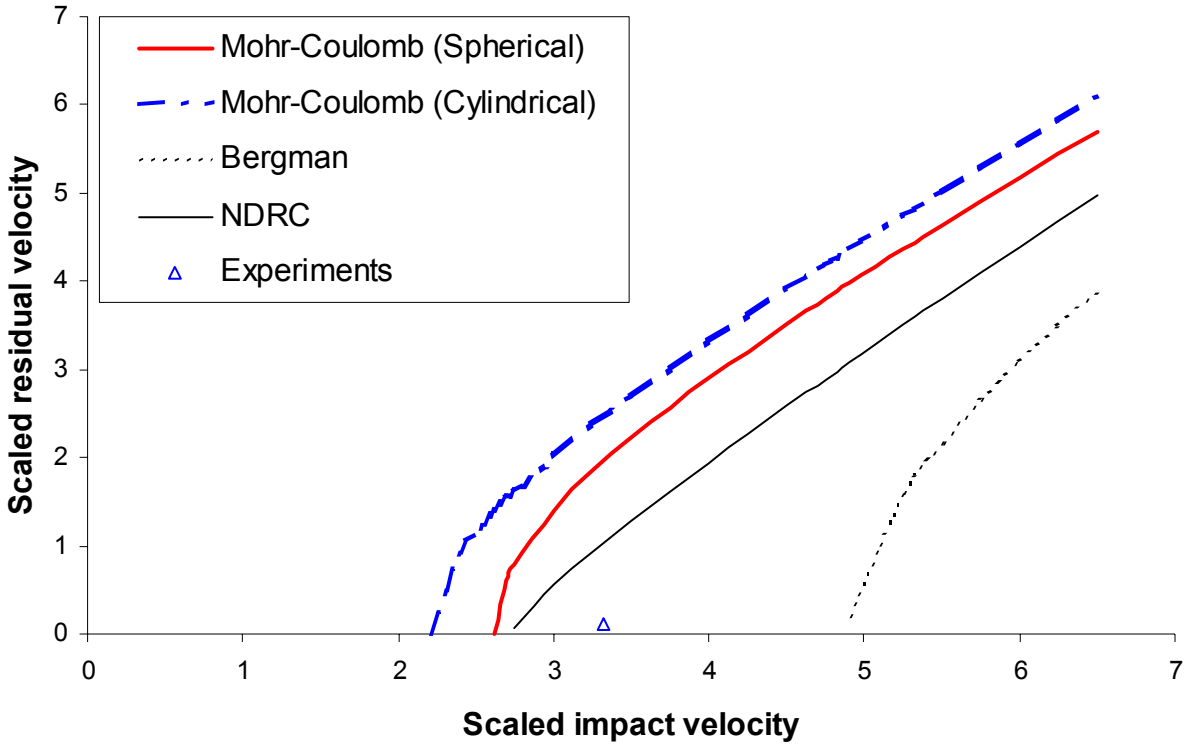

Figure 4.6 Residual velocity as a function of impact velocity for H = 6.

In this case, we only have one data point, and it is difficult to draw any conclusions.

4.3.5 H = 7 (Hanchak et al [16])

Table 4.6 Different experiments against thin concrete targets (Hanchak et al [16]).

Target		Projectile				
Comp str. [MPa]	Thickness [cm]	Mass [kg]	Diameter [mm]	v_0 [m/s]	v_{exit} [m/s]	Remarks
48	17.8	0.5	25.4	301	0	
48	17.8	0.5	25.4	360	67	
48	17.8	0.5	25.4	381	136	
48	17.8	0.5	25.4	434	214	
48	17.8	0.5	25.4	606	449	
48	17.8	0.5	25.4	746	605	
48	17.8	0.5	25.4	749	615	
48	17.8	0.5	25.4	1058	947	
140	17.8	0.5	25.4	376	0	
140	17.8	0.5	25.4	482	0	
140	17.8	0.5	25.4	443	171	
140	17.8	0.5	25.4	522	265	
140	17.8	0.5	25.4	587	368	
140	17.8	0.5	25.4	743	544	
140	17.8	0.5	25.4	998	842	

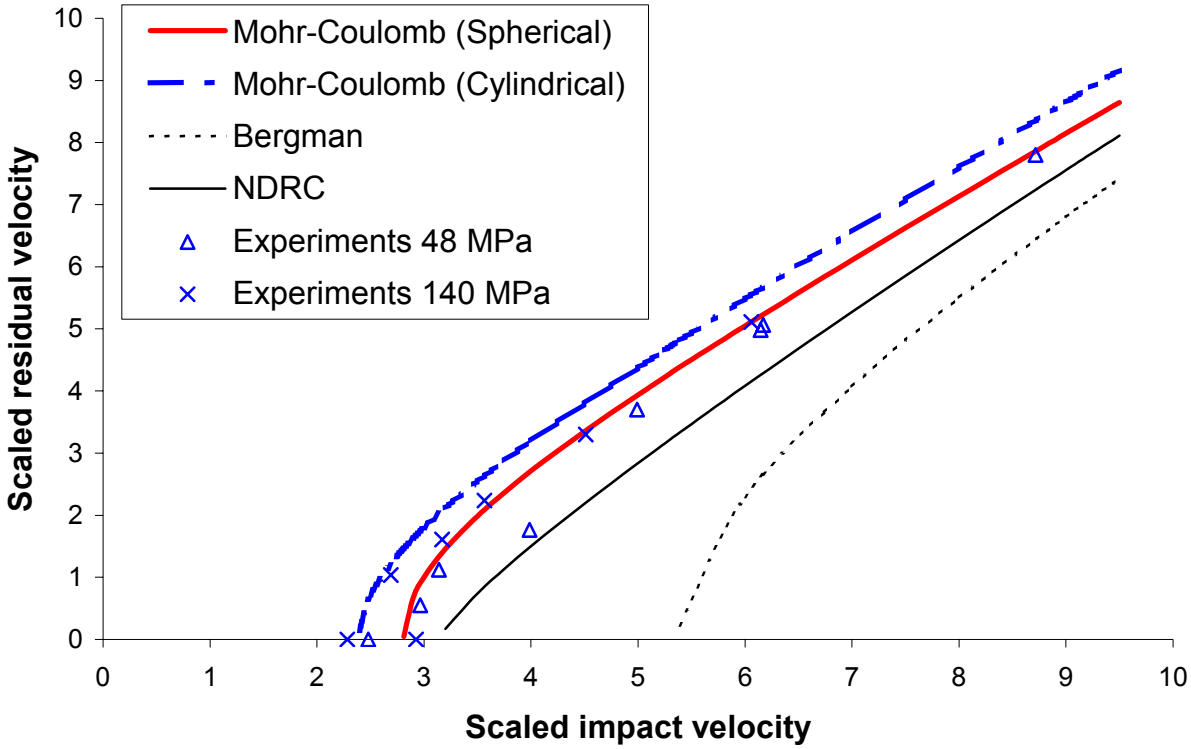

Figure 4.7 Residual velocity as a function of impact velocity for H = 7.

For high impact velocities, it seems that the residual velocity calculated with the spherical cavity expansion model gives a better agreement with the experiments, while there is a little more scattering in the experimental data near the ballistic limit. The experiments against 140 MPa concrete seems to agree better with the cylindrical CE model, while the experiments against 48 MPa concrete agree more with the spherical CE model. The reason for this observation is, however, not clear at the moment, and there is a need for further investigation to clarify this question.

4.4 Discussion

In the comparison made in the previous section, the FFI-model seems to predict the residual velocity better than the model in the Norwegian fortification handbook, although the present model also gives a little under-prediction near the ballistic limit. This may be due to the fact that our model does not take the brittle behaviour of the target material into account.

It is not obvious whether the spherical or cylindrical cavity expansion approach gives the best representation of the target resistance. The comparison in this chapter shows that the residual velocity in most experiments is between the results from the two CE approaches.

5 THICKNESS TO PREVENT PERFORATION

When building protective structures, it is important to know how to prevent perforation of KE projectiles. In this chapter, the cavity expansion approach will be used to determine the required thickness to prevent perforation. The CE-model will be compared to existing methods found in the literature, and to some of the experiments discussed in the previous chapter.

5.1 Cavity expansion approach

Using the CE-model, the thickness to prevent perforation can be found numerically from

$$\int_{X_2}^{H_p} \alpha(X)dX = \frac{2}{\pi}\frac{M}{N}\ln\left(1+\frac{N}{M}\frac{V_2^2}{S}\right) \tag{5.1}$$

where V_2 is given by either Equation (2.13) or (2.16).

5.2 Existing methods from the literature

Some of the existing formulas for required target thickness are related to the penetration depth in semi-infinite targets in the following way

$$H_p = aP_\infty + b \tag{5.2}$$

The parameters *a* and *b* for some actual formulas are given in Table 5.1.

Table 5.1 Constants in Equation (5.2).

Formula	*a*	*b*
NDRC [17]	1.24	1.32
Degen [18]	1.29	0.69
Hughes [19]	1.58	1.4
Petry [20]	2	0

It is very important to note that the thickness to prevent perforation in Equation (5.2) is related to the corresponding penetration depth formula in semi-infinite targets, i.e. P_∞ is not identical for all formulas listed in Table 5.1.

Some other formulas, which are defined in a different way, were also discussed in Teland [1]:

Adeli & Amin [21]

$$H_p = 0.906 + 0.3214NV - 0.0106(NV)^2 \tag{5.3}$$

CEA-EDF [22]

$$H_p = \frac{0.82}{dv^{0.25}}\left(\frac{\sigma_c}{\rho_t}\right)^{0.25} V \tag{5.4}$$

Chang [23]

$$H_p = \frac{2.79}{v^{0.25}} V \tag{5.5}$$

Bergman [11,24]

$$H_p = 1.19 \cdot 10^{-3} N \frac{d^{0.725}\sigma_c^{0.075}}{m^{0.242}} V^{1.15} \tag{5.6}$$

Table 5.2 Experiments near the ballistic limit compared to empirical formulas (m = 0.5 kg; d = 25 mm).

H	v_0	v_{exit}	σ_c	Thickness to prevent perforation (H_p)								
				FFI	A/A	CEA	Chang	Berg man	Hughes	NDRC	Degen	Petry
2	135	10	200	1.9-2.2	1.4	1.7	1.4	0.8	2.4	2.9	2.3	8.6
	140	0	600	1.6-1.9	1.2	1.5	0.8	0.5	2.1	2.8	2.2	9.1
6	547	20	140	11.2-13.3	2.8	5.5	4.8	4.5	6.7	7.7	7.4	36.9
7	301	0	48	5.6-8.0	2.7	5.1	5.1	3.8	3.8	5.4	5.0	21.7
	360	67	48	8.6-11.3	2.9	5.9	5.8	4.7	4.7	6.5	6.1	25.6
	482	0	140	8.4-11.1	2.7	4.9	4.2	3.8	3.8	6.5	6.1	32.2
	443	171	140	6.2-9,6	2.6	4.6	4.0	3.5	3.5	5.9	5.5	30.2

The thickness to prevent perforation as shown in Table 5.2 should in most cases be somewhat larger than the thickness used in the experiment because the projectile actually perforated the target in the experiments. The two values for the FFI-model are calculated from spherical and cylindrical CET, respectively. We see from Table 5.2 that the FFI-model gives higher values for the perforation thickness than found experimentally, but our model predicts the perforation thickness better than most of the other formulas. For the experiments with $H = 2$, the FFI-model predicts H_p between 1.9 and 2.2 for a 200 MPa concrete and H_p between 1.6 and 1.9 for a 600 MPa concrete. For the experiments with $H = 7$, our model predicts a scaled thickness to prevent perforation between 5.6 and 11.3 for a 48 MPa concrete, while the predicted thickness for a 140 MPa concrete is between 6.2 and 11.1. It should be mentioned that we should have had more experiments in this comparison to obtain a better statistical foundation for our comparison.

It is difficult to show the results in Table 5.2 graphically, because most of the empirical formulas involved are not dimensionally correct, and therefore it is impossible to show the

variation of the scaled thickness to prevent perforation as a general function of the scaled impact velocity.

Our model should be "safe" to use when constructing protective structures, since it overpredicts the required wall thickness by a couple of projectile diameters.

6 PENETRATION INTO THIN TARGETS

In some cases, the concrete wall is too thin to be regarded as semi-infinite, but the thickness is larger than the perforation thickness so the projectile will stop inside the target. In these situations, the penetration depth P_{thin} is found from

$$\int_{X_2}^{P_{thin}} \alpha(X)dX = \frac{2}{\pi}\frac{M}{N}\ln\left(1+\frac{N}{M}\frac{V_2^2}{S}\right) \tag{6.1}$$

where V_2 is given by either Equation (2.13) or (2.16).

From [12], the penetration depth into thin targets is given by

$$P_{thin}^{US} = \frac{1}{H_s - H_p}\left[P_{NDRC}\left(H - H_p\right) + H_p\left(H_s - H\right)\right] \qquad H_s \le H \le H_p \tag{6.2}$$

where H_s is the thickness to prevent spalling discussed in the next chapter, and H_p is the thickness to prevent perforation calculated from Equation (5.2) using the values for the NDRC formula. In Figure 6.1, the penetration depth relative to penetration depth into semi-infinite targets as a function of scaled target thickness is shown for a 25.4 mm projectile with impact velocity of 300 m/s into a 48 MPa concrete target. The CE approach is compared to the NDRC model in Equation (6.2).

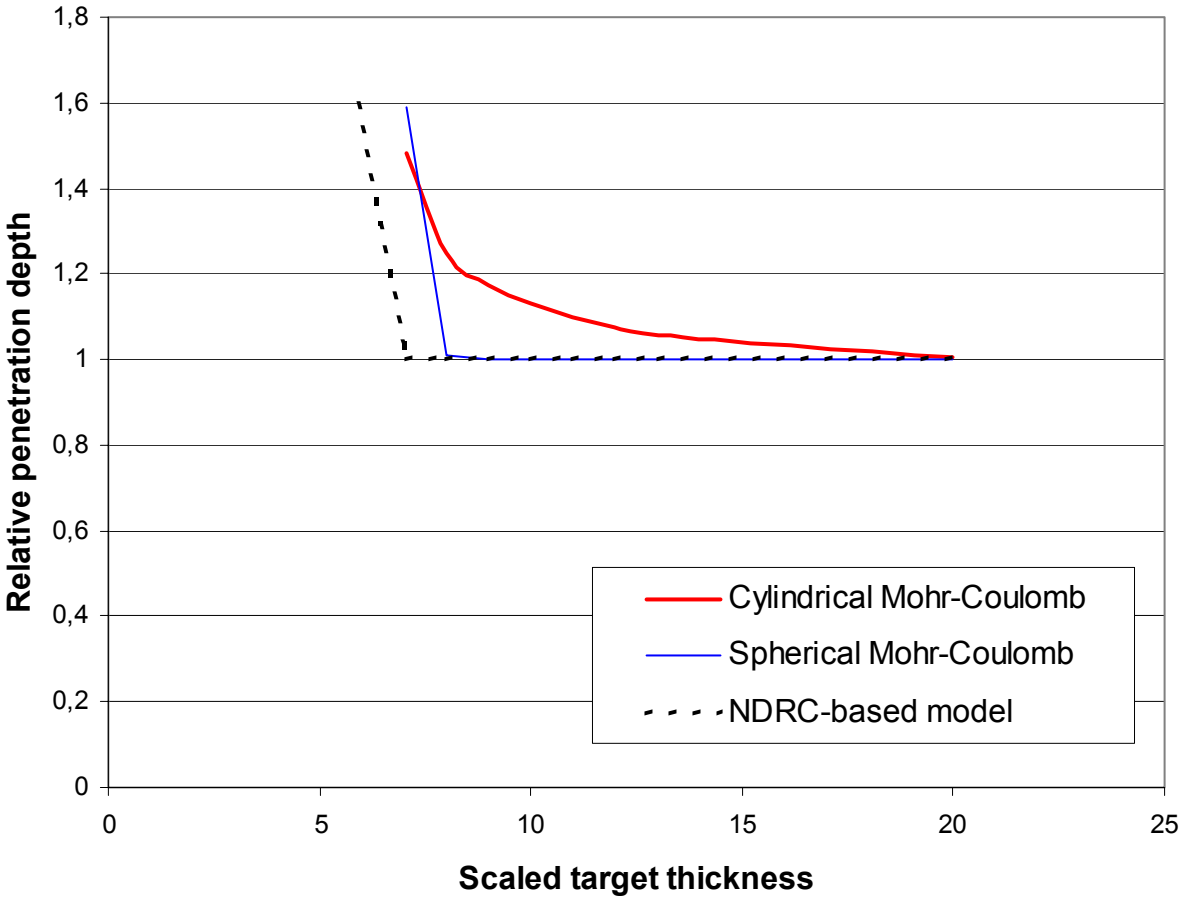

Figure 6.1 *Relative penetration depth as function of scaled target thickness for a 25.4 mm projectile into a 48 MPa concrete target with an impact velocity of 300 m/s.*

The spherical CE approach seems to be in better agreement with the empirical formula (6.2) for target thickness larger than the "spalling thickness" (see the next chapter for discussion), i.e. the target is considered to be semi-infinite if no damage is visible on the rear side of the concrete target. For thinner targets, the only difference between the spherical CE model and the empirical NDRC model is the perforation thickness.

7 THICKNESS TO PREVENT SPALLING

The thickness to prevent spalling is not found directly from the cavity expansion approach presented in this report, but is included here for completeness. Formula (7.1), taken from [12], gives an estimate of the scaled target thickness to prevent spalling.

$$H_s = 1{,}375 P_{\mathrm{NDRC}} + 2 \tag{7.1}$$

In Figure 7.1, this formula is compared to the cavity expansion solutions for penetration depth into semi-infinite targets and the required thickness to prevent perforation for a 75 mm projectile. Even though the cavity expansion approach in this report can not be used to

calculate the spalling thickness, Figure 7.1 shows that the spalling thickness compared to the CE results for perforation and penetration depth is reasonable.

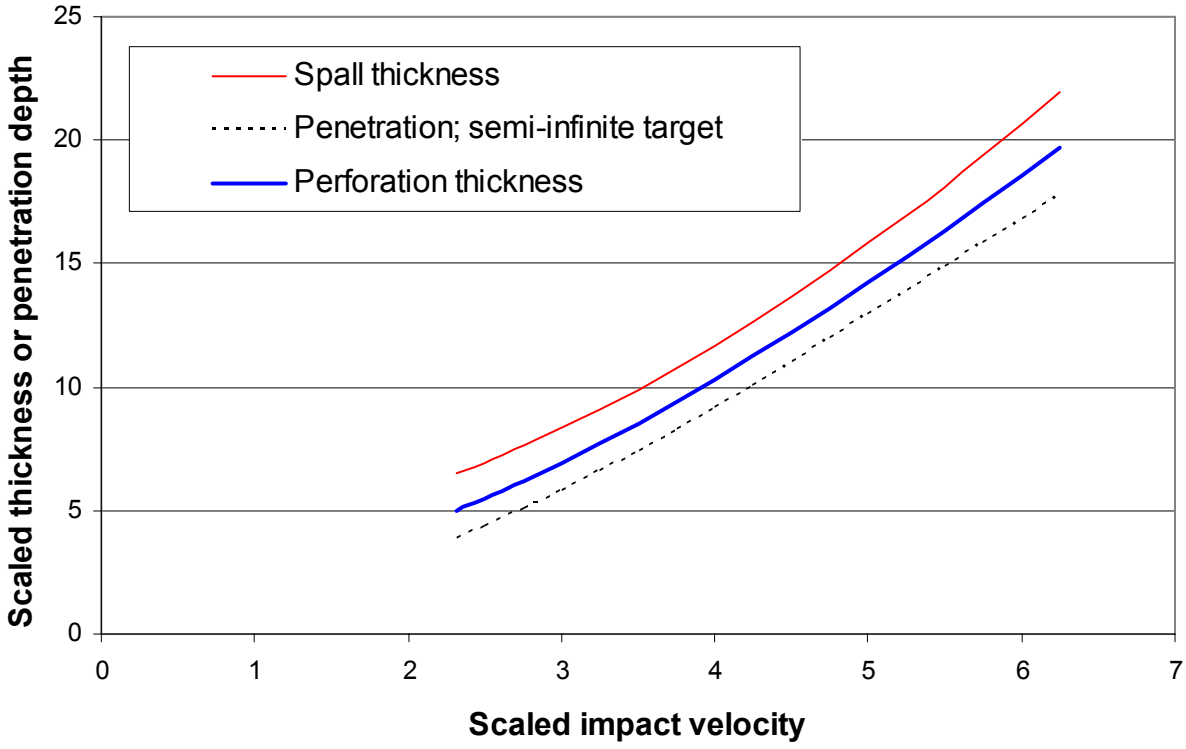

Figure 7.1 *Scaled thickness to prevent spalling and perforation as a function of scaled impact velocity compared to the penetration depth into semi-infinite targets for 75 mm projectiles.*

8 CONCLUSIONS

The cavity expansion approach for penetration of rigid projectiles into semi-infinite concrete targets has been further developed to calculate perforation problems as well. In addition, a Mohr-Coulomb based material model has been used to give an estimate of the target resistance. The comparison to different empirical models shows that the CE approach gives a better agreement to the experiments than the other models.

Bergman's formula is underpredicting both the ballistic limit and the residual velocity compared to all experiments analysed in this report. The NDRC model gives acceptable results near the ballistic limit against thin targets ($H = 2$). In this case, the residual velocity is estimated too low compared to the experiments. Against thicker targets, the CE model gives the best results.

The perforation thickness calculated from the CE model is in agreement with the experimental values, although we should have more experiments to obtain a better statistical foundation. Compared to the existing empirical models, the CE model is shown to be good. Especially

against thick concrete targets ($H = 7$), the other models predict a low thickness to prevent perforation, which is not desirable for dimensioning purposes.

For penetration into targets that can not be considered as semi-infinite, the CE model is compared to an empirical model based on the NDRC model. The qualitative behaviour using spherical CE is almost identical compared to the NDRC based model, where the only difference is the value of the perforation thickness.

The cavity expansion models presented here, in addition to the models for semi-infinite targets, form a complete collection of powerful analytical tools for analysing normal impact of rigid projectiles against concrete targets.

References

(1) Teland J A (1997): A review of empirical equations for missile impact effects on concrete, FFI/RAPPORT-97/05856

(2) Forrestal M J, Altman B S, Cargile J D, Hanchak S J (1994): An empirical equation for penetration depth of ogive-nose projectiles into concrete targets , Int. J. Impact Eng. 15, 4, 395-405.

(3) Sjøl H, Teland J A (1999): Prediction of concrete penetration using Forrestal's formula, FFI/RAPPORT-99/04415

(4) Teland J A, Sjøl H (2000): Penetration into concrete by truncated projectiles, FFI/RAPPORT-2000/05292

(5) Teland J A, Sjøl H (2000): Boundary effects in penetration into concrete, FFI/RAPPORT-2000/05414.

(6) Sjøl H, Teland J A (2001): Boundary effects in penetration of rigid projectiles into "High Performance Concrete" (HPC) Targets, Proceedings from the 10th international symposium on interaction of the effects of munitions with structures, San Diego, USA, 7. – 11. May 2001.

(7) Littlefield D L, Anderson Jr C E, Partom Y, Bless S J (1997): The penetration of steel targets finite in radial extent, Int J. Impact Engng 19, 1, 49-62.

(8) Warren T L, Poormon K L, Penetration of 6061-T6511 aluminum targets by ogive-nosed VAR 4340 steel projectiles at oblique angles: experiments and simulations, Int. J. Imp. Engng. Vol 25, pp. 993-1022, 2001

(9) Sjøl H, Teland J A, Kaldheim Ø (1998) Penetrasjon i betong med 12 mm prosjektiler, FFI/NOTAT-98/04392 (in Norwegian)

(10) Børvik T, Langseth M, Hopperstad O S, Malo K A (1998):Ballistic penetration of steel plates, Proceedings from "Transient loading and response of structures", NTNU Trondheim, Norway, pp 241 - 272, May 25 - 27 1998

(11) Norwegian Fortification handbook (1990) (in Norwegian)

(12) Design and Analysis of Hardened Structures to Conventional Weapons Effects, Army TM5-8551/Air Force AFPAM 32-1147(I)/Navy NAVFAC P-1080/DSWA DAHSCWEMAN-97, Washington DC, 1998.

(13) Darrigade A, Buzaud E (1999): High performance concrete: A numerical and experimental study, International Ballistics Symposium 1999.

(14) Svinsås E, O'Caroll C, Wentzel C M, Carlberg A (2001): Benchmark trial to provide validation data for modeling, Proceedings from the 10th international symposium on

interaction of the effects of munitions with structures, San Diego, USA, 7. – 11. May 2001.

(15) Magnusson J, Unosson M, Carlberg A (2001): High Performance Concrete (HPC); Field experiments and production, FOI-R-0256-SE, FOI, Sweden

(16) Hanchak S J, Forrestal M J, Young E R, Ehrgott J Q (1992): Perforation of concrete slabs with 48 MPa and 140 MPa unconfined compressive strengths, Int J Impact Engng, Vol 12, No1, pp 1-8

(17) NDRC: Effects of impact and explosion, summary of technical Report of division 2, National Defence Research Commitee, Vol 1, Washington D C

(18) Degen P P (1980): Perforation of reinforced concrete slabs by rigid missiles, Journal of the structural division, Vol. 106, No ST7, pp 1623 - 1642

(19) Hughes G (1984): Hard missile impact on reinforced concrete, *Nuclear Engineering and Design* **77**, 23-35

(20) Hellström K-G (1986): Jämförelse mellan några olika former för beräkning av projectilers inträngning i betong, FortF rapport C6, Eskilstuna, Sweden (in Swedish)

(21) Adeli H, Amin M (1985): Local effects of impactors on concrete structures, Nuclear Engineering and design 88, pp 301-317

(22) Barriaud R S, Sokolovsky A, Gueraud Dulac J R, Labrot R (1978): Local behaviour of reinforced concrete walls under missile impact, Nuclear Engineering and design, Vol 45, pp. 457 – 469

(23) ChangW S (1981): Impact of solid missiles on concrete barriers, Journal of the structural division, Vol 107, No ST2, pp 257 - 271

(24) Bergman S G A (1950): Inträngning av panserbrytande projectiler och bomber i armerad betong, FortF Rapport B2, Stockholm, Sweden (in Swedish)

(25) Partom Y (1996): Static cavity expansion model for partially confined targets, Proceedings of 16th Int Symposium on Ballistics, pp. 571-580

A CALCULATION OF REDUCTION FACTOR

When the projectile is near a free surface, the resistance force is reduced. The reduction factor is calculated as the ratio between the target resistance in a finite material and the target resistance in a semi-infinite material. In a finite material, the situation is illustrated in Figure A.1. Near the cavity, the material behaves plastically, while the material far from the cavity is still elastic. The stresses and strains in the material are calculated using continuity and boundary conditions at the interfaces between the different regions.

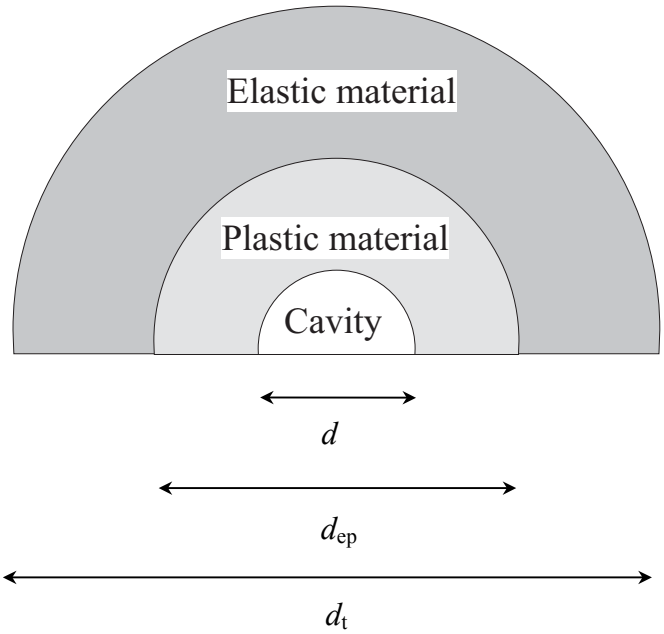

Figure A.1 The physical problem in cavity expansion is to find the pressure at the cavity surface (r=d) as the cavity expands, while known boundary conditions apply at the elastic-plastic boundary ($r=d_{ep}$) and the elastic boundary ($r=d_t$).

In general, the stress-strain relationship can be written as

$$\sigma_{ij} = \lambda \varepsilon_{kk} \delta_{ij} + 2G\varepsilon_{ij} \tag{A.1}$$

where

$$\lambda = \frac{2G\nu}{1-2\nu} \tag{A.2}$$

The strain-displacement relationship is given by

Spherical coordinates (spherical symmetry):

$$\varepsilon_{rr} = \frac{\partial u_r}{\partial r} \quad \varepsilon_{\theta\theta} = \varepsilon_{\phi\phi} = \frac{u_r}{r} \quad \varepsilon_{r\theta} = \varepsilon_{\phi\theta} = \varepsilon_{\theta r} = 0 \tag{A.3}$$

Cylindrical coordinates (radial symmetry):

$$\varepsilon_{rr} = \frac{\partial u_r}{\partial r} \quad \varepsilon_{\theta\theta} = \frac{u_r}{r} \quad \varepsilon_{r\theta} = 0 \tag{A.4}$$

A.1 Mises material modell

A.1.1 Spherical CET

The boundary conditions are given by:

$$\begin{aligned}
&\sigma_{rr}^{p}(d) = -p_r \\
&\sigma_{rr}^{e}(d_{ep}) = \sigma_{rr}^{p}(d_{ep}) \\
&\sigma_{rr}^{e}(d_{ep}) - \sigma_{\theta\theta}(d_{ep}) = -Y \\
&\sigma_{rr}^{e}(d_t) = 0 \\
&u_r^{e}(d_{ep}) = u_r^{p}(d_{ep})
\end{aligned} \tag{A.5}$$

The equation of motion is given by:

$$\frac{\partial \sigma_{rr}^{e}}{\partial r} + 2\frac{\sigma_{rr}^{e} - \sigma_{\theta\theta}^{e}}{r} = 0 \tag{A.6}$$

giving

$$\frac{\partial^2 u_r}{\partial r^2} + \frac{2}{r}\frac{\partial u_r}{\partial r} - \frac{2}{r^2}u_r = 0 \tag{A.7}$$

The solution of (A.7) is found to be

$$u_r(r) = K_1 r + \frac{K_2}{r^2} \tag{A.8}$$

The radial stress in the elastic region is then given by

$$\sigma_{rr}^{e}(r) = (\lambda + 2G)\frac{\partial u_r}{\partial r} + 2\lambda\frac{u_r}{r} = (\lambda + 2G)\left(K_1 - \frac{2K_2}{r^3}\right) + 2\lambda\left(K_1 + \frac{K_2}{r^3}\right) \tag{A.9}$$

Using the boundary condition $\sigma_{rr}^{e}(d_t) = 0$ gives the following relationship between K_1 and K_2.

$$K_1 = \frac{4G}{3\lambda + 2G}\frac{K_2}{d_t^3} \tag{A.10}$$

At the elastic-plastic interface ($r = d_{ep}$), we have $\sigma_{rr}^{e} - \sigma_{\theta\theta}^{e} = -Y$ [2].

$$\begin{aligned} \sigma_{rr}^{e}(d_{ep}) &= 4GK_2\left[\frac{1}{d_t^3} - \frac{1}{d_{ep}^3}\right] \\ \sigma_{\theta\theta}^{e}(r) &= \left(2\lambda + 2G\right)\frac{u_r}{r} + \lambda\frac{\partial u_r}{\partial r} = 2GK_2\left[\frac{2}{d_t^3} + \frac{1}{r^3}\right] \end{aligned} \tag{A.11}$$

giving

$$\begin{aligned} &\sigma_{rr}^{e}(d_{ep}) - \sigma_{\theta\theta}^{e}(d_{ep}) = 2GK_2\left[\frac{2}{d_t^3} - \frac{2}{d_{ep}^3} - \frac{2}{d_t^3} - \frac{1}{d_{ep}^3}\right] = -\frac{6K_2}{d_{ep}^3}G = -Y \\ &K_2 = \frac{d_{ep}^3 Y}{6G} \end{aligned} \tag{A.12}$$

Inserting this into (A.10) gives

$$K_1 = \frac{2Y}{3\left(3\lambda + 2G\right)}\left(\frac{d_{ep}}{d_t}\right)^3 \tag{A.13}$$

In the plasticity region, we have

$$\frac{\partial \sigma_{rr}^{p}}{\partial r} + 2\frac{\sigma_{rr}^{p} - \sigma_{\theta\theta}^{p}}{r} = 0 \tag{A.14}$$

using a Mises yield criterion ($\sigma_{rr}^{p} - \sigma_{\theta\theta}^{p} = -Y$) combined with the boundary condition $\sigma_{rr}^{p}(d) = -p_r$, we have

$$\sigma_{rr}^{p}(r) = 2Y\ln\left(\frac{r}{d}\right) - p_r \tag{A.15}$$

Continuity in the radial stress at the elastic-plastic interface ($r = d_{ep}$) gives

$$4GK_2\left[\frac{1}{d_t^3} - \frac{1}{d_{ep}^3}\right] = 2Y\ln\left(\frac{d_{ep}}{d}\right) - p_r \tag{A.16}$$

[2] Stresses are here negative in compression and positive in tension.

$$p_r = 2Y \ln\left(\frac{d_{ep}}{d}\right) + \frac{2Y}{3}\left[1 - \left(\frac{d_{ep}}{d_t}\right)^3\right] \tag{A.17}$$

d_{ep}/d_t as a function of d_t/d is found from conservation of mass (see for instance Partom [25]):

$$\left(\frac{d_{ep}}{d}\right)^3 = \frac{d_{ep}}{3u_r(d_{ep})} \tag{A.18}$$

where

$$u_r(d_{ep}) = K_1 d_{ep} + \frac{K_2}{d_{ep}^2} = Y\left[\frac{2}{9\lambda + 6G}\left(\frac{d_{ep}}{d_t}\right)^3 + \frac{1}{6G}\right] d_{ep} \tag{A.19}$$

Solving (A.19) with respect to d_{ep}/d_t gives the following equation:

$$\frac{2Y}{3\lambda + 2G}\left(\frac{d_{ep}}{d_t}\right)^6 + \frac{Y}{2G}\left(\frac{d_{ep}}{d_t}\right)^3 - \left(\frac{d}{d_t}\right)^3 = 0 \tag{A.20}$$

This finally yields

$$\left(\frac{d_{ep}}{d_t}\right)^3 = \frac{1}{4}\frac{1+\nu}{1-2\nu}\left(\sqrt{1 + \frac{16G}{Y}\frac{1-2\nu}{1+\nu}\left(\frac{d}{d_t}\right)^3} - 1\right) \tag{A.21}$$

A.1.2 Cylindrical CET

The boundary conditions in this case are given by Equation (A.5). The equation of motion using cylindrical coordinates is

$$\frac{\partial \sigma_{rr}}{\partial r} + \frac{\sigma_{rr} - \sigma_{\theta\theta}}{r} = 0 \tag{A.22}$$

giving

$$\frac{\partial^2 u_r}{\partial r^2} + \frac{1}{r}\frac{\partial u_r}{\partial r} - \frac{1}{r^2}u_r = 0 \tag{A.23}$$

The solution of (A.23) is on the form

$$u_r(r) = K_1 r + \frac{K_2}{r} \tag{A.24}$$

The radial stress in the elastic region is given by

$$\sigma_{rr}^e(r) = (\lambda + 2G)\frac{\partial u_r}{\partial r} + \lambda\frac{u_r}{r} = (\lambda + 2G)\left(K_1 - \frac{K_2}{r^2}\right) + \lambda\left(K_1 + \frac{K_2}{r^2}\right) \tag{A.25}$$

$$\sigma_{\theta\theta}^e(r) = K_2\left[(\lambda + 2G)\left(\frac{G}{\lambda + G}\frac{1}{d_t^2} + \frac{1}{r^2}\right) + \lambda\left(\frac{G}{\lambda + G}\frac{1}{d_t^2} - \frac{1}{r^2}\right)\right] \tag{A.26}$$

Using the boundary condition $\sigma_{rr}^e(d_t) = 0$ gives the following relationship between K_1 and K_2.

$$K_1 = \frac{G}{\lambda + G}\frac{K_2}{d_t^2} \tag{A.27}$$

At the elastic-plastic interface ($r = d_{\text{ep}}$), we have $\sigma_{rr}^e - \sigma_{\theta\theta}^e = -Y$, giving

$$K_2 = \frac{d_{ep}^2 Y}{4G} \tag{A.28}$$

Inserting this into Equation (A.27) gives

$$K_1 = \frac{Y}{4(\lambda + G)}\left(\frac{d_{ep}}{d_t}\right)^2 \tag{A.29}$$

In the plasticity region, the equation of motion is given by

$$\frac{\partial \sigma_{rr}^p}{\partial r} + \frac{\sigma_{rr}^p - \sigma_{\theta\theta}^p}{r} = 0 \tag{A.30}$$

using a Mises yield criterion ($\sigma_{rr}^p - \sigma_{\theta\theta}^p = -Y$) combined with the boundary condition $\sigma_{rr}^p(d) = -p_r$, we obtain

$$\sigma_{rr}^p(r) = Y\ln\left(\frac{r}{d}\right) - p_r \tag{A.31}$$

Continuity in the radial stress at the elastic-plastic interface ($\sigma_{rr}^p(d_{ep}) = \sigma_{rr}^e(d_{ep})$) gives

$$p_r = \frac{Y}{2}\left[1 - \left(\frac{d_{ep}}{d_t}\right)^2 + \ln\left(\frac{d_{ep}}{d}\right)^2\right] \tag{A.32}$$

$d_{\text{ep}}/d_{\text{t}}$ as a function of d_{t}/d is found from conservation of mass:

$$\left(\frac{d_{ep}}{d}\right)^2 = \frac{d_{ep}}{2u_r(d_{ep})} \tag{A.33}$$

Solving (A.33) with respect to d_{ep}/d_t gives:

$$\left(\frac{d_{ep}}{d_t}\right)^2 = \frac{1}{2(1-2\nu)}\left[\sqrt{1+\frac{8G}{Y}2(1-2\nu)\left(\frac{d}{d_t}\right)^2}-1\right] \tag{A.34}$$

A.2 Mohr-Coulomb material model

A.2.1 Spherical CET

The elastic solution is given by

$$u_r(r) = K_2\left[\frac{4G}{3\lambda+2G}\frac{r}{d_t^3}+\frac{1}{r^2}\right] \tag{A.35}$$

which is similar to the Mises solution, except that the constant K2 will be different due to different boundary conditions. The elastic radial stress is given by:

$$\sigma_{rr}^e(r) = 4GK_2\left[\frac{1}{d_t^3}-\frac{1}{r^3}\right] \tag{A.36}$$

For Mohr-Coulomb materials, the yield stress depends on the pressure in the following way:

$$\begin{aligned}&\sigma_{\theta\theta}^p - \sigma_{rr}^p = Y_0 + \beta p\\ &p = \frac{1}{3}\left(2\sigma_{\theta\theta}^p + \sigma_{rr}^p\right)\end{aligned} \tag{A.37}$$

This gives the following relationship between $\sigma_{\theta\theta}^p$ and σ_{rr}^p:

$$\sigma_{\theta\theta}^p = \frac{3Y_0}{(3-2\beta)} + \frac{(3+\beta)}{(3-2\beta)}\sigma_{rr}^p = Y + \alpha\sigma_{rr}^p \tag{A.38}$$

The equation of motion in the plasticity region is given by

$$\frac{\partial\sigma_{rr}^p}{\partial r} + 2\frac{\sigma_{rr}^p - \sigma_{\theta\theta}^p}{r} = 0 \tag{A.39}$$

Inserting the Mohr-Coulomb yield stress, we obtain

$$\sigma_{rr}^{p} - \sigma_{\theta\theta}^{p} = -Y + (1-\alpha)\sigma_{rr}^{p} \tag{A.40}$$

giving the following equation:

$$\frac{\partial \sigma_{rr}^{p}}{\partial r} + 2\frac{(1-\alpha)\sigma_{rr}^{p} - Y}{r} = 0 \tag{A.41}$$

Separation of variables gives

$$\frac{d\sigma_{rr}^{p}}{Y - (1-\alpha)\sigma_{rr}^{p}} = 2\frac{dr}{r} \tag{A.42}$$

which after integration gives

$$\frac{1}{\alpha - 1}\ln\left[Y + (\alpha - 1)\sigma_{rr}^{p}\right] = 2\ln r + k \tag{A.43}$$

and

$$\sigma_{rr}^{p} = \tilde{k} r^{2(\alpha-1)} - \frac{Y}{\alpha - 1} \tag{A.44}$$

The boundary condition $\sigma_{rr}^{p}(d) = -p_r$ gives

$$\tilde{k} = \left[\frac{Y}{\alpha - 1} - p_r\right] d^{-2(\alpha-1)} \tag{A.45}$$

resulting in the following expression for the radial plastic stress:

$$\sigma_{rr}^{p}(r) = -p_r\left(\frac{r}{d}\right)^{2(\alpha-1)} + \frac{Y}{\alpha - 1}\left[\left(\frac{r}{d}\right)^{2(\alpha-1)} - 1\right] \tag{A.46}$$

Inserting the values for Y and α, gives

$$\sigma_{rr}^{p}(r) = -p_r\left(\frac{r}{d}\right)^{\left(\frac{6\beta}{3-2\beta}\right)} + \frac{Y_0}{2\beta}\left[\left(\frac{r}{d}\right)^{\left(\frac{6\beta}{3-2\beta}\right)} - 1\right] \tag{A.47}$$

Continuity in the shear stress at the elastic-plastic interface
$(\sigma_{rr}^{p}(d_{ep}) - \sigma_{\theta\theta}^{p}(d_{ep}) = \sigma_{rr}^{e}(d_{ep}) - \sigma_{\theta\theta}^{e}(d_{ep}))$ gives:

$$\frac{3\beta}{3-2\beta}p_r\left(\frac{d_{ep}}{d}\right)^{\left(\frac{6\beta}{3-2\beta}\right)}-\frac{3Y_0}{3-2\beta}\left[\left(\frac{d_{ep}}{d}\right)^{\left(\frac{6\beta}{3-2\beta}\right)}-1\right]-\frac{3Y_0}{3-2\beta}=-\frac{6K_2}{d_{ep}^3}G \tag{A.48}$$

resulting in

$$K_2=d_{ep}^3\frac{Y_0-\beta p_r}{2G(3-2\beta)}\left(\frac{d_{ep}}{d}\right)^{\left(\frac{6\beta}{3-2\beta}\right)} \tag{A.49}$$

Continuity in the radial stress at the elastic-plastic interface ($\sigma_{rr}^p(d_{ep})=\sigma_{rr}^e(d_{ep})$) gives

$$-p_r\left(\frac{d_{ep}}{d}\right)^{\left(\frac{6\beta}{3-2\beta}\right)}+\frac{Y_0}{2\beta}\left[\left(\frac{d_{ep}}{d}\right)^{\left(\frac{6\beta}{3-2\beta}\right)}-1\right]=4G\left[\frac{1}{d_t^3}-\frac{1}{d_{ep}^3}\right]d_{ep}^3\frac{Y_0-\beta p_r}{2G(3-2\beta)}\left(\frac{d_{ep}}{d}\right)^{\left(\frac{6\beta}{3-2\beta}\right)} \tag{A.50}$$

After some calculations, we obtain:

$$p_r=\frac{Y_0}{\beta}\left[1-\frac{\left(\frac{d}{d_{ep}}\right)^{\left(\frac{6\beta}{3-2\beta}\right)}}{\left[1-\frac{2\beta}{3-2\beta}\left\{\left(\frac{d_{ep}}{d_t}\right)^3-1\right\}\right]}\right] \tag{A.51}$$

The elastic plastic diameter d_{ep} is here unknown. By using conservation of mass, d_{ep}/d_t as a function of d/d_t is found:

$$\left(\frac{d_{ep}}{d}\right)^3=\frac{d_{ep}}{3u_r(d_{ep})} \tag{A.52}$$

where

$$u_r(d_{ep})=\left[\frac{4G}{3\lambda+2G}\frac{d_{ep}}{d_t^3}+\frac{1}{d_{ep}^2}\right]\frac{d_{ep}^3\left(Y_0-\beta p_r\right)}{2G(3-2\beta)}\left(\frac{d_{ep}}{d}\right)^{\left(\frac{6\beta}{3-2\beta}\right)} \tag{A.53}$$

and

$$Y_0 - \beta p_r = Y_0 \frac{\left(\frac{d}{d_{ep}}\right)^{\left(\frac{6\beta}{3-2\beta}\right)}}{\left[1 - \frac{2\beta}{3-2\beta}\left\{\left(\frac{d_{ep}}{d_t}\right)^3 - 1\right\}\right]} \tag{A.54}$$

giving

$$\left(\frac{d}{d_t}\right)^3\left[\left(\frac{d_t}{d_{ep}}\right)^3 - \frac{2\beta}{3-2\beta}\left(1-\left(\frac{d_t}{d_{ep}}\right)^3\right)\right] = \frac{Y_0}{2G(3-2\beta)}\left[\frac{2(1-2\nu)}{3+2\nu}\left(\frac{d_{ep}}{d_t}\right)^3 + 1\right] \tag{A.55}$$

$$\left(\frac{d}{d_t}\right)^3\left[1 - \frac{2\beta}{3-2\beta}\left(\left(\frac{d_{ep}}{d_t}\right)^3 - 1\right)\right] = \frac{Y_0}{2G(3-2\beta)}\left[\frac{2(1-2\nu)}{3+2\nu}\left(\frac{d_{ep}}{d_t}\right)^6 + \left(\frac{d_{ep}}{d_t}\right)^3\right] \tag{A.56}$$

Ordering the terms gives the following equation to calculate d_{ep}/d_t:

$$\frac{Y_0}{G}\frac{(1-2\nu)}{(3+2\nu)}\left(\frac{d_{ep}}{d_t}\right)^6 + \left[\frac{Y_0}{2G} + 2\beta\left(\frac{d}{d_t}\right)^3\right]\left(\frac{d_{ep}}{d_t}\right)^3 - 2\beta\left(\frac{d}{d_t}\right)^3 = 0 \tag{A.57}$$

Solving with respect to d_{ep}/d_t finally gives:

$$\left(\frac{d_{ep}}{d_t}\right)^3 = \frac{1-2\nu}{4(3+2\nu)}\left[\sqrt{\left(1 + \frac{4\beta(3+2\nu)^2}{(1-2\nu)^2}\frac{G}{Y_0}\left(\frac{d}{d_t}\right)^3\right)^2 + \frac{32\beta(3+2\nu)^3}{(1-2\nu)^3}\frac{G}{Y_0}\left(\frac{d}{d_t}\right)^3} - 1 - \frac{2\beta(3+2\nu)^2}{(1-2\nu)^2}\frac{G}{Y_0}\left(\frac{d}{d_t}\right)^3\right] \tag{A.58}$$

A.2.2 Cylindrical CET

The elastic solution is given by

$$u_r(r) = K_2\left[\frac{G}{\lambda + G}\frac{r}{d_t^2} + \frac{1}{r}\right] \tag{A.59}$$

which is similar to the Mises solution, except that the constant K2 will be different due to different boundary conditions. The elastic radial stress is given by:

$$\sigma_{rr}^e(r) = \left[2G\frac{1}{d_t^2} + (\lambda + 2G)\frac{1}{r^2}\right]K_2 \tag{A.60}$$

For Mohr-Coulomb materials, we have

$$\sigma_{\theta\theta}^{p} - \sigma_{rr}^{p} = Y_0 + \beta p$$
$$p = \frac{1}{3}\left(\sigma_{\theta\theta}^{p} + \sigma_{rr}^{p}\right) \tag{A.61}$$

After some calculations, similar to the spherical Mohr-Coulomb case described in Section A.2.1, we obtain the following expression for the radial plastic stress:

$$\sigma_{rr}^{p}(r) = -p_r\left(\frac{r}{d}\right)^{\left(\frac{2\beta}{3-\beta}\right)} + \frac{3Y_0}{2\beta}\left[\left(\frac{r}{d}\right)^{\left(\frac{2\beta}{3-\beta}\right)} - 1\right] \tag{A.62}$$

Continuity in the shear stress at the elastic-plastic interface ($\sigma_{rr}^{p}(d_{ep}) - \sigma_{\theta\theta}^{p}(d_{ep}) = \sigma_{rr}^{e}(d_{ep}) - \sigma_{\theta\theta}^{e}(d_{ep})$) gives:

$$K_2 = d_{ep}^2 \frac{3Y_0 - 2\beta p_r}{4G(3-\beta)}\left(\frac{d_{ep}}{d}\right)^{\left(\frac{2\beta}{3-\beta}\right)} \tag{A.63}$$

Continuity in the radial stress at the elastic-plastic interface ($\sigma_{rr}^{p}(d_{ep}) = \sigma_{rr}^{e}(d_{ep})$) finally gives:

$$p_r = \frac{3Y_0}{2\beta}\left[1 - \frac{\left(\frac{d}{d_{ep}}\right)^{\left(\frac{2\beta}{3-\beta}\right)}}{\left[1 - \frac{\beta}{3-\beta}\left\{\left(\frac{d_{ep}}{d_t}\right)^2 - 1\right\}\right]}\right] \tag{A.64}$$

Again, conservation of mass enables us to find an expression for d_{ep}:

$$\left(\frac{d_{ep}}{d}\right)^2 = \frac{d_{ep}}{2u_r(d_{ep})} \tag{A.65}$$

where

$$u_r(d_{ep}) = \left[\frac{G}{\lambda + G}\frac{d_{ep}}{d_t^2} + \frac{1}{d_{ep}}\right]\frac{d_{ep}^2\left(3Y_0 - 2\beta p_r\right)}{4G(3-\beta)}\left(\frac{d_{ep}}{d}\right)^{\left(\frac{2\beta}{3-\beta}\right)} \tag{A.66}$$

and

$$3Y_0 - 2\beta p_r = 3Y_0 \frac{\left(\frac{d}{d_{ep}}\right)^{\left(\frac{2\beta}{3-\beta}\right)}}{1-\frac{\beta}{3-\beta}\left(\left(\frac{d_{ep}}{d_t}\right)^2 - 1\right)} \tag{A.67}$$

Combining Equations (A.65) – (A.67), gives the following equation to calculate d_{ep}/d_t:

$$\frac{3Y_0}{4G}(1-2\nu)\left(\frac{d_{ep}}{d_t}\right)^4 + \left[\frac{3Y_0}{4G} + \beta\left(\frac{a}{d_t}\right)^2\right]\left(\frac{d_{ep}}{d_t}\right)^2 - 3\left(\frac{d}{d_t}\right)^2 = 0 \tag{A.68}$$

Solving with respect to d_{ep}/d_t gives:

$$\left(\frac{d_{ep}}{d_t}\right)^2 = \frac{-\left[\frac{3Y_0}{4G} + \beta\left(\frac{d}{d_t}\right)^2\right] + \sqrt{\left[\frac{3Y_0}{4G} + \beta\left(\frac{d}{d_t}\right)^2\right]^2 + 9\frac{Y_0}{G}(1-2\nu)\left(\frac{d}{d_t}\right)^2}}{\frac{3Y_0}{2G}(1-2\nu)} \tag{A.69}$$

DISTRIBUTION LIST

FFIBM **Dato:** 6. august 2003

RAPPORTTYPE (KRYSS AV)	RAPPORT NR.	REFERANSE	RAPPORTENS DATO
X RAPP ☐ NOTAT ☐ RR	2001/05786	FFIBM/766/130	6. august 2003
RAPPORTENS BESKYTTELSESGRAD		ANTALL EKS UTSTEDT	ANTALL SIDER
Unclassified		26	48
RAPPORTENS TITTEL		FORFATTER(E)	
PERFORATION OF CONCRETE TARGETS		SJØL Henrik, TELAND Jan Arild	
FORDELING GODKJENT AV FORSKNINGSSJEF		FORDELING GODKJENT AV AVDELINGSSJEF:	
Bjarne Haugstad		Jan Ivar Botnan	

EKSTERN FORDELING

ANTALL	EKS NR	TIL
1		Forsvarsbygg
1		v/ Helge Langberg
1		v/ Tore Børvik
1		Jim Sheridan
		DSTL
		Missiles and Countermeasures Dept.
		Room G056, Building A2
		Ively Road
		Farnborough, Hants., Gu14 0LX
		England
1		Jaap Weerheijm
		TNO
		Lange Kleiweg 137
		P. O. Box 45
		2280 AA Rijswijk
		Nederland
1		Johan Magnusson
		FOI
		Weapons and Protection
		14725 Tumba
		Sverige

INTERN FORDELING

ANTALL	EKS NR	TIL
9		FFI-Bibl
1		Adm direktør/stabssjef
1		FFIE
1		FFISYS
1		FFIBM
1		FFIN
2		Jan Arild Teland, FFIBM
2		Henrik Sjøl, FFIBM
1		Ove Dullum, FFIBM
1		John F Moxnes, FFIBM
		Elektronisk fordeling:
		FFI-veven
		Lars Kvifte (LKv), FFIBM
		Bjarne Haugstad (BjH), FFIBM
		Svein Rollvik (SRo), FFIS
		Knut B. Holm (KBH), FFIBM
		Svein Martinussen(SEM), FFIBM
		Haakon Fykse (HFy), FFIBM

FFI-K1 Retningslinjer for fordeling og forsendelse er gitt i Oraklet, Bind I, Bestemmelser om publikasjoner for Forsvarets forskningsinstitutt, pkt 2 og 5. Benytt ny side om nødvendig.